WOODHEAD PUBLISHING SERIES IN BIOMATERIALS

SILK-BASED BIOMATERIALS FOR TISSUE ENGINEERING, REGENERATIVE AND PRECISION MEDICINE

SECOND EDITION

Edited by
SUBHAS C. KUNDU
RUI L. REIS

ELSEVIER

Chapter 5

Structure and properties of spider and silkworm silks for tissue engineering and medicine

Gustavo V. Guinea[1,2,3], Manuel Elices[1,2,3], José Pérez-Rigueiro[1,2,3] and Gustavo R. Plaza[1,2,3]

[1]*Departamento de Ciencia de Materiales, ETSI Caminos, Canales y Puertos, Madrid, Spain,* [2]*Center for Biomedical Technology, Madrid, Spain,* [3]*Universidad Politécnica de Madrid, Madrid, Spain*

5.1 Introduction

Tissue engineering is one of the most vital areas of interdisciplinary scientific research, in which the development of appropriate materials for use as scaffolds is critical. The ideal scaffold for a tissue-engineered biological substitute has to simulate the form and function of the pertinent extracellular matrix (ECM). Silk scaffolds are promising because they can promote cell attachment and proliferation; they are biocompatible, degradable, and functionalizable; and some of their properties (e.g., fiber diameter, strength or pore size) are easily tunable.

This chapter is devoted to silk fibers, as a primary component of silk scaffolds and other medical components. The purpose is to familiarize the reader with natural silk fibers either from silkworms or spiders and with their synthetic counterparts. Emphasis is given to mechanical properties, as they are significant in scaffold design.

To this end, Section 5.2 is devoted to silk fibers' composition, production (spinning), and microstructure. Section 5.3 deals with their mechanical performance—mainly inferred from tensile tests—under different environments, focusing on the influence of water and temperature. Section 5.4 is concerned with relationships between structure and mechanical properties; here, some models intending to replicate the mechanical behavior of the fiber are briefly summarized. Finally, biomimetic approaches for making synthetic silk fibers are outlined, studying regenerated silkworm silk and genetically engineered (or bioinspired) spider silk. The chapter ends with some examples of medical applications.

Silk-Based Biomaterials for Tissue Engineering, Regenerative and Precision Medicine.
DOI: https://doi.org/10.1016/B978-0-323-96017-5.00010-8

5.2 Silk fibers

This section reviews the composition and production of silk fibers, and how these two factors influence the unique microstructural features of these materials.

5.2.1 Chemical composition

Silks are singular among protein fibers produced exclusively by animals belonging to the phylum *Arthropoda*. Silks serve various biological functions in a group with such a rich ecology, including providing shelter, protecting the offspring, and capturing prey [1]. Despite its widespread distribution in the lineage, it has not been possible to establish whether silk production is the result of a unique evolutionary event or whether its presence in different groups of arthropods is the consequence of several independent processes [2]. However, it is apparent that, independently from their evolutionary origin, silks share several standard features, starting with their composition; in this regard, it was soon realized [1,3] that a defining mark of silks is a large proportion of the short-chain amino acids glycine and alanine.

The advent of more powerful analytical techniques led to a significant increase in knowledge of the composition of silks, albeit focused mainly on the two most studied silk types: silkworm (*Bombyx mori*) silk and major ampullate silk (MAS) from a few orb-weaving spider species (i.e., *Nephila clavipes* and *Argiope trifasciata*, among others). *B. mori* silk is made up of two proteins, known collectively as fibroins, which differ in their molecular weight: a heavy fibroin chain of approximately 350 kDa and a light fibroin chain of 25 kDa. Both proteins appear in a 1:1 proportion and are linked through a disulfide bond [4]. The complete sequencing of the heavy-chain protein [5] revealed an extensive repetition of the −Gly−Ala−Gly−Ala−Gly−Ser− a motif that, as explained below, has a significant influence on the microstructure of the material. The biochemical characterization of MAS revealed that it is made up of two large (approximately 300 kDa) proteins labeled spidroin 1 and spidroin 2 [6], which are characterized by extensive repetitions of distinct motifs along the sequence. Spidroin 1 shows the motifs −Gly−Ala− (although in this protein, it does not form the extensive repeats that appear in *B. mori* silk), −Gly−Gly−X− (with X = Leu, Gln, or Tyr), and $-A_n-$ (polyalanine runs). Although spidroin 2 also shows the motif $-A_n-$, it differs from spidroin 1 in the high content of proline, which appears in the motif −Gly−Pro−Gly−. It has been found that, despite strong arguments in favor of a considerable evolutionary divergence among silk sequences [7], MAS sequences have been conserved for over 120 million years [8], indicating an extreme evolutionary pressure which has not been identified yet [9].

5.2.2 Spinning

A solution of proteins susceptible to forming fibers does not represent the end of the story, as indicated by the painstaking efforts to spin regenerated silk fibers from previously dissolved silkworm silk fibroins [10]. Although some basic details are still missing, the spinning processes of both silkworm and MAS show parallels that allow at least a general description of the route that leads from a protein solution to the fiber formation.

As with the comparison of the sequences between *B. mori* and spider MAS, and despite the uncertainty of a possible common origin, both glandular systems show remarkable similarities. Thus, glands are divided into two (*Nephila edulis*) [11] or three (*B. mori*) [12] parts. Silk proteins are produced in the proximal region of the gland by dedicated epithelial cells that line the lumen and are stored in the distal regions. A third region in the *B. mori* gland is related to the production of sericin proteins, which act as glue for maintaining the structural integrity of the cocoon. More significant differences are found when analyzing the duct that links the distal part of the gland with the spinneret. Thus, the *N. edulis* duct [11] is composed of three different limbs whose cross-sectional areas decrease in the distal direction and, immediately before reaching the spinneret, passes through an organ (valve) controlled by at least two muscles. This sophisticated system is probably related to the control exerted by the spider on its silk properties and contrasts with the more superficial anatomy of a silkworm silk duct [13].

The organization of the silk proteins in the gland and the conformational changes that lead to the solid fiber are still debatable. Two basic essential (Fig. 5.1), not necessarily incompatible, models attempt to account for this process. The liquid crystal model [15] finds support from results obtained *in vivo* and assumes that proteins in the gland adopt a rod-like conformation and form a liquid crystalline nematic structure. The molecule's axis is aligned with the walls of the gland and physicochemical changes in the gland lead to the formation of β-nanocrystals that renders insoluble fibers, while preserving the overall organization exhibited in the liquid crystalline phase. The micellar model [16] hypothesizes that the alternating hydrophobic and hydrophilic patches in the silk proteins lead to micelles forming globular structures. These globular structures are elongated in the duct, leading to fiber formation. Independent from the precursor phase that the protein adopts in the gland, it is accepted that shear stresses exerted on the protein solution are critical for prompting the solidification process [12]. The presence of proton pumps in the duct [11] suggests that pH may play a significant role in the process, an assumption further supported by the presence of pH conformational switches in the sequence of silk proteins [17,18].

As indicated above, some of the most significant differences between *B. mori* and spider spinning processes are related to the control exerted by the animal on the process. It has been found that spiders can tune the

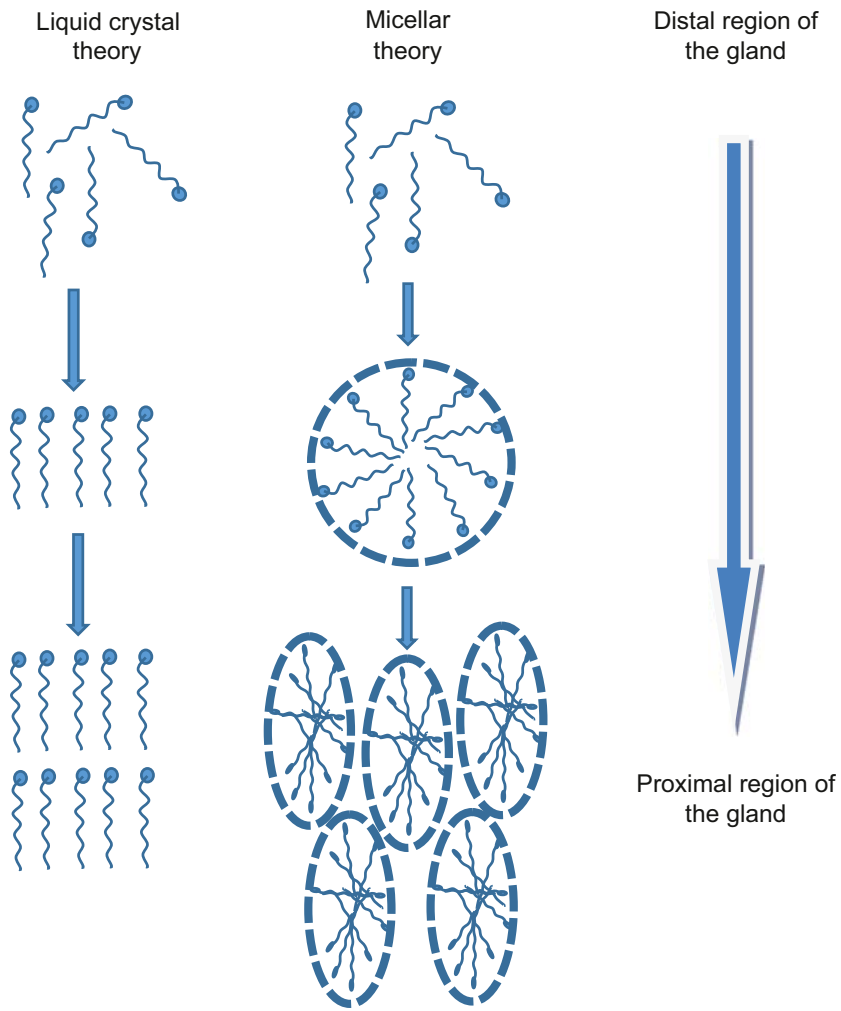

FIGURE 5.1 The liquid crystal and the micellar models [14]. *Based on Heim M, Keerl D, Scheibel T. Spider silk: from soluble protein to extraordinary fiber. Angew Chem Int Ed Engl 2009;48(20):3584–96.*

properties of the fiber by controlling the spinning force (see Section 5.3.2), probably with the use of the valve [19], so that a vast range of mechanical properties characterized by the corresponding range of stress–strain curves, fitted to its immediate requirements can be produced [20]. In contrast, the spinning system in *B. mori* seems to lack a comparable step, leading to fibers with uniform properties when obtained directly from the silkworm without a degumming process [21,22].

5.2.3 Fiber microstructure

Unveiling the microstructural organization of silk from the atomic to the macroscopic scale probably represents the most significant challenge for an overall understanding of the material. Applying some of the most sophisticated characterization techniques has allowed information to be gained on some essential aspects of silk, but a comprehensive model is still sought. In this regard, silk's single most defining microstructural character is the presence of a crystalline phase embedded in a noncrystalline or amorphous matrix [23]. The crystalline phase is evident from the X-ray diffraction (XRD) analysis of the fibers and consists of nanocrystals that appear as a consequence of the piling up of β-pleated sheets [24]. In this regard, β-nanocrystals are found both in silkworms [25] and in spider silk [26], and their presence is related to the motifs of sequence −GAGAGS− and −poly-A_n−, respectively. In the absence of chemical cross-links between silk protein chains, the nanocrystals provide the necessary structural integrity to the fiber. Its formation during the spinning process is considered as the critical step that converts the protein solution into a solid fiber.

The characterization of spider silk by Raman spectroscopy [27] has identified several secondary structures, including β-turns, 3_{10} helices, and β-sheets. A significant fraction of an unordered or random coil phase was determined using Raman spectroscopy. Our understanding of the amorphous phase is much poorer than that of the crystalline one. Independent from its detailed microstructure, the analysis of the behavior of silk fibers in water of both spider [28] and silkworm silk [29] supports a model [30], sometimes referred to as the double lattice model (see Section 5.4.2), in which an extensive lattice of hydrogen bonds is superimposed on the lattice formed by the protein chains. However, linking this rough model with the details of the sequence and the conformation of the proteins has proven a formidable task.

An intriguing feature of spider silk is the possibility of sustaining significant microstructural changes related to varying loading and/or environmental conditions. nuclear magnetic resonance (NMR) studies [31] have identified that the motif −Gly−Gly−X−, which appears in spidroin 1, shows a significant degree of conformational freedom. In particular, this motif has been related to the supercontraction effect, a considerable shrinkage of the fiber when exposed to water or high relative humidity environments [28], which plays a critical role in spider silk performance [32]. Although supercontraction appears in basal lineages of spiders [33], its extent and its influence on the mechanical behavior of the material are more apparent in the orb-web spinning spiders. The possibility of reversibly modifying the crystalline fraction of spider silk has found experimental support from XRD studies, which show an increase in crystallinity when the fiber sustains large deformations [34].

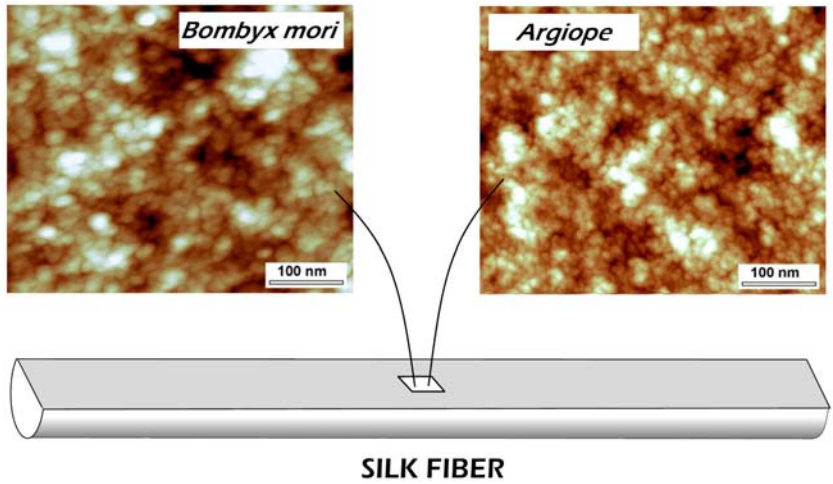

FIGURE 5.2 High-resolution images, obtained by atomic force microscopy, of *Bombyx mori* and *Argiope trifasciata* silk fibers [38].

The characterization of silks at more considerable scale lengths in an attempt to unveil their supramolecular organization from the nanometer to the macroscopic scale has rendered a minimal number of definite results. Several models based on low-resolution atomic force microscopy (AFM) studies assume that proteins are organized at mesoscopic scales forming nano- or micro-fibrils [35,36]. However, transmission X-ray microscopy [37] and high-resolution AFM [38] have failed to find a fibrillar microstructure in spider silk. In particular, high-resolution AFM (Fig. 5.2) has shown a structure made up of nanometer-size globules, which differ in size depending on the analyzed silk [38]. Fractographic studies have not found features of a fibrillar microstructure either [39] since silk fracture surfaces appear relatively flat and no fibrils can be identified. However, neutron scattering and small-angle XRD [40,41] suggest the presence of some long-range organization in spider silk, although the exact nature of this ordering and its relationship with silk sequence are far from clear.

5.3 Mechanical properties

Tensile tests mainly characterize the mechanical performance of silk fibers because of their simplicity and ability to incorporate different environments (temperature and humidity). This fact is crucial since, due to the natural variability of silk fibers, the control of environmental conditions makes possible the settlement of a common ground for comparison and analysis.

5.3.1 Tensile tests

Natural silks are characterized by some outstanding mechanical properties, namely high tensile strength and high elongation at failure, that endow them with the most significant work of fracture of any known material [4,15,42].

Tensile tests are most appropriate for obtaining the mechanical characteristics of most materials, especially so for fibers because of their simplicity. Samples are elongated between two grips while force and extension are measured. Absolute force-displacement ($F-\Delta$) plots are converted into engineering (or nominal) stress–strain ($s-e$) curves (Fig. 5.3) by dividing force (F) by the initial cross-sectional area (A_0) and displacement ($\Delta = L - L_0$) by the initial length (L_0):

$$s = F/A_0 \quad \text{and} \quad e = \Delta/L_0 \tag{5.1}$$

Although engineering values are convenient for samples with small elongation before breaking (e.g., $<10\%$, like most ordinary artificial materials), the large deformations accommodated by silks recommend the use of true stress–strain curves (σ, ε), where force and displacement values are calculated with the instantaneous cross-sectional area (A) and length (L) at each point of the test. Thus, true values are defined by:

$$\sigma = F/A \quad \text{and} \quad d\varepsilon = dL/L \tag{5.2}$$

which leads to:

$$\varepsilon = \ln\left(L/L_0\right) = \ln(1 + e) \tag{5.3}$$

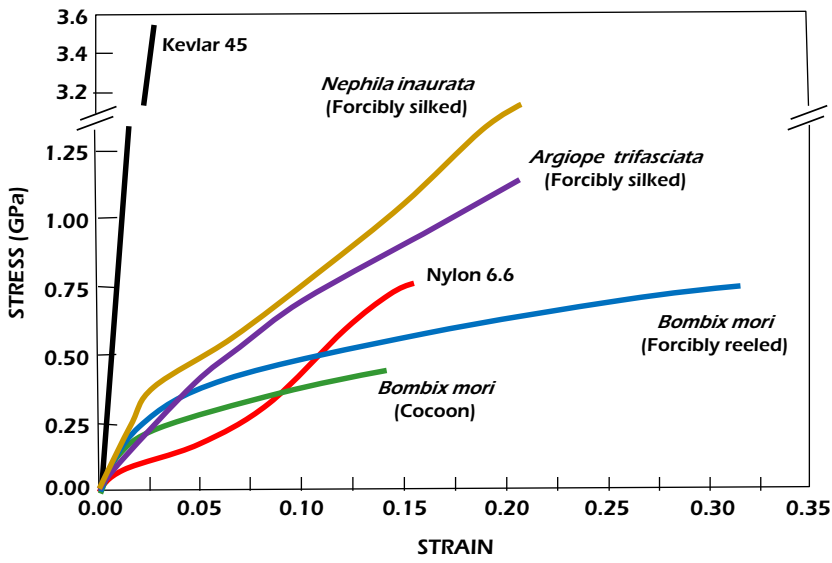

FIGURE 5.3 Stress–strain curves for different fibers.

Instantaneous cross-section can be readily computed under the hypothesis of constant volume during deformation $AL = A_0L_0$, [43] yielding:

$$\sigma = F/A = \left(F/A_0\right)\left(L/L_0\right) = s(1+e) \tag{5.4}$$

Mechanical parameters like the initial elastic modulus (E), the tensile strength (σ_u), and elongation at break (ε_u) are directly obtained from the stress−strain curve ($\sigma-\varepsilon$).

Silk fibers display true tensile strengths comparable to high-performance steel and polymeric fibers, such as Kevlar or poly(p-phenylene-2,6-benzobisoxazole) (PBO) while keeping an unrivaled high strain at break (Table 5.1). High strengths and strains at break combine in MAS to yield an unbeatable capacity for absorbing energy—also called tenacity or resilience, quantified by the area under the stress−strain curve (see Fig. 5.3 and Table 5.1)—that enables spiders to effectively intercept and catch their prey. Key to this ability is a large hysteresis cycle of more than 50% shown by silk fibers during loading−unloading cycles that impart a large capacity of energy dissipation since, otherwise, prey would bounce off the orb web. Both viscoelasticity and irreversible deformation account for the large hysteresis, probably produced by frictional forces among segments of protein chains.

Mechanical properties of silks are time-dependent, and fibers creep when subjected to constant loading or relax under imposed deformation (Fig. 5.4A) [50]. Stress relaxation does not decay to zero and reaches a constant value within approximately 1 day (similar to the spider-web life cycle). Silk fibers show an increase in the initial modulus of elasticity, yield stress, tensile strength, and breaking strain when tested at higher strain rates (Fig. 5.4B).

Fig. 5.5 shows the results of dynamic-mechanical thermal analysis tests conducted in natural MAS [51]. The sample is subjected to an alternating sinusoidal strain in these tests while the stress is continuously recorded. Temperature usually varies from freezing conditions up to sample melting or degradation. Dynamic behavior is characterized by the *storage modulus* (Fig. 5.5A), the ratio between in-phase stress and strain, and the *loss tangent* (Fig. 5.5B), that is, the tangent of the phase difference between strain and stress waves.

The peaks in the storage modulus and loss tangent curves shown in Fig. 5.5 suggest that relaxation is associated with interactions at different molecular levels (hydrocarbon−hydrocarbon, water−amide, and amide−amide) as well as possible crystallization at higher temperatures. Fig. 5.5A also shows that MAS has good heat resistance, failing mechanically only beyond $\sim$250°C.

5.3.2 Spider and silkworm fibers

MAS fibers can either be gathered from the web (radii, frame, and mooring lines) or the safety line (dragline), all of them labeled as naturally spun (NS), or collected directly from the gland of an immobilized spider by a process

TABLE 5.1 Average values of mechanical properties of silk fibers and high-performance synthetic fibers.

Fiber type	Density (g/cm^3)	Tensile stress (MPa)	Breaking strain (%)	Resilience (MJ/m^3)	References
Silk fibers	1.34				
Argiope trifasciata					
Naturally spun (NS)		780	26	90	[44]
Forced silked (FS)		1110	17	110	[45]
Maximum supercontraction (Ms)		990	81	240	[45]
Nephila inaurata					
FS		1800	26	240	[46]
Ms		1480	69	270	[46]
Nephila clavipes					
FS		1200	17	110	[47]
Bombix mori					
FS		730	11	50	[48]
Commercial		600	23	90	[49]
Polymeric fibers					
PBO	1.60	5800	2.5	70	

(*Continued*)

TABLE 5.1 (Continued)

Fiber type		Density (g/cm^3)	Tensile stress (MPa)	Breaking strain (%)	Resilience (MJ/m^3)	References
	Kevlar 49	1.44	3000	2.7	50	[49]
	Nylon 6,6 (HT)	1.14	750	18	70	[49]
	PET (HT)	1.90	800	7	30	[49]
Silk fibers		7.85				
	Strand		1800	5	70	[49]
	Piano wire		3000	1.5	25	[49]

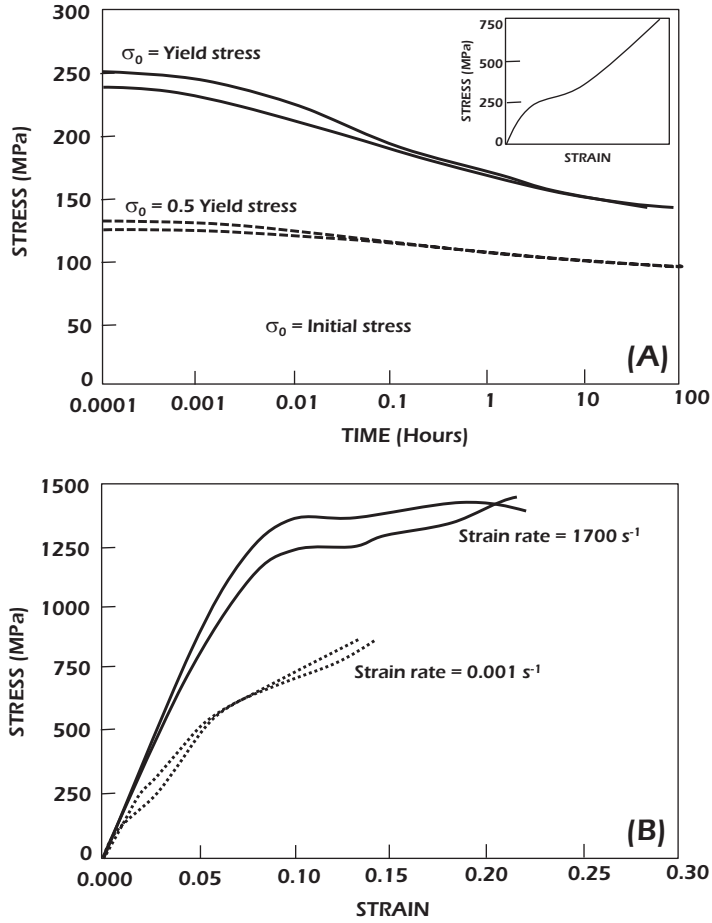

FIGURE 5.4 (A) Stress relaxation of major ampullate silk (MAS) fibers from *A. trifasciata*. The initial stresses were chosen to be either the conventional yield stress or 0.5 times the yield stress [50]. (B) Influence of the strain rate on the stress–strain curves of MAS fibers from *A. trifasciata* [50].

called forced silking (FS). Although the quantity of silk retrieved in both cases is small, the FS procedure permits obtaining large ($\sim$1 m) continuous fibers.

The tensile properties of NS and FS fibers are different as depicted in Fig. 5.6A. NS fibers show a large variability, customarily attributed to a biological production system that adapts to the immediate requirements of the environment [22,44,52–54]. FS fibers, in contrast, display low variability and differ considerably from NS. FS fibers are stiffer, more reproducible, and show smaller deformations and higher stresses at breaking than NS, differences that can reasonably be attributed to the different processing.

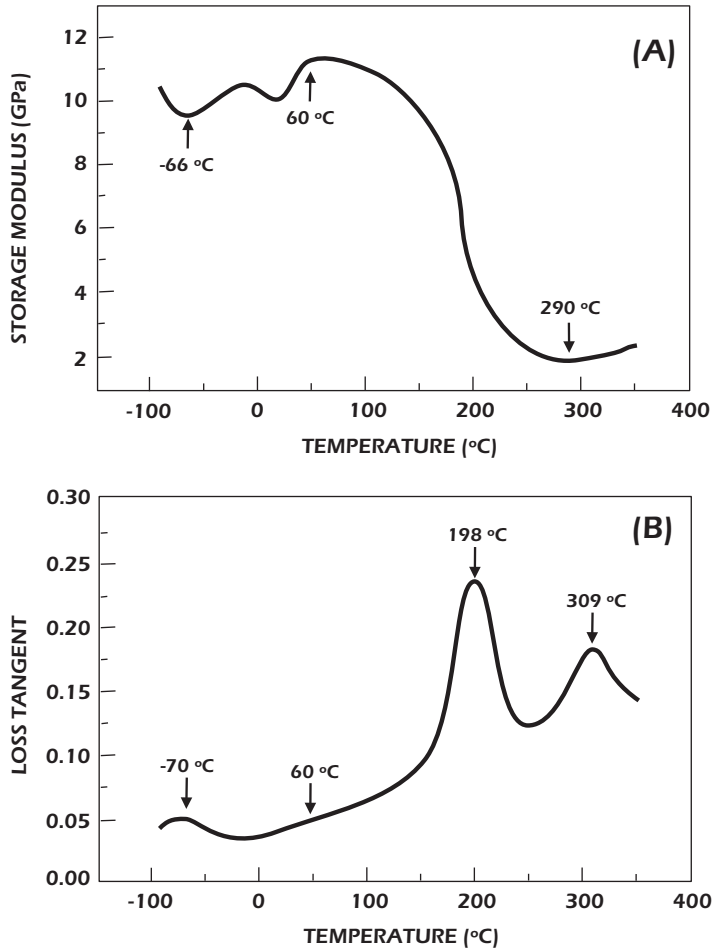

FIGURE 5.5 Dynamic-mechanical thermal analysis of major ampullate silk fibers from *N. edulis*. (A) Storage modulus and (B) loss tangent. *Reproduced from Yang ZT, Liivak O, Seidel A, Laverde G, Zax DB, Jelinski LW. Supercontraction and backbone dynamics in spider silk: C-13 and H-2 NMR studies. J Am Chem Soc 2000;122(37):9019–25.*

Measurement of the silking force has made it possible to correlate the silking stress—the stress on the fiber during spinning—and silk fiber tensile properties [20]. Very reproducible fibers are obtained when silking stress is constant, making the fibers stiffer or more compliant depending on the silking stress level (Fig. 5.7). FS fibers produced with silking stresses close to the yield limit are stiffer than NS like the ones shown in Fig. 5.7A. As the silking stress decreases, the stiffness of FS fibers reduces to resemble the NS range and it is possible to obtain fibers even more compliant than those

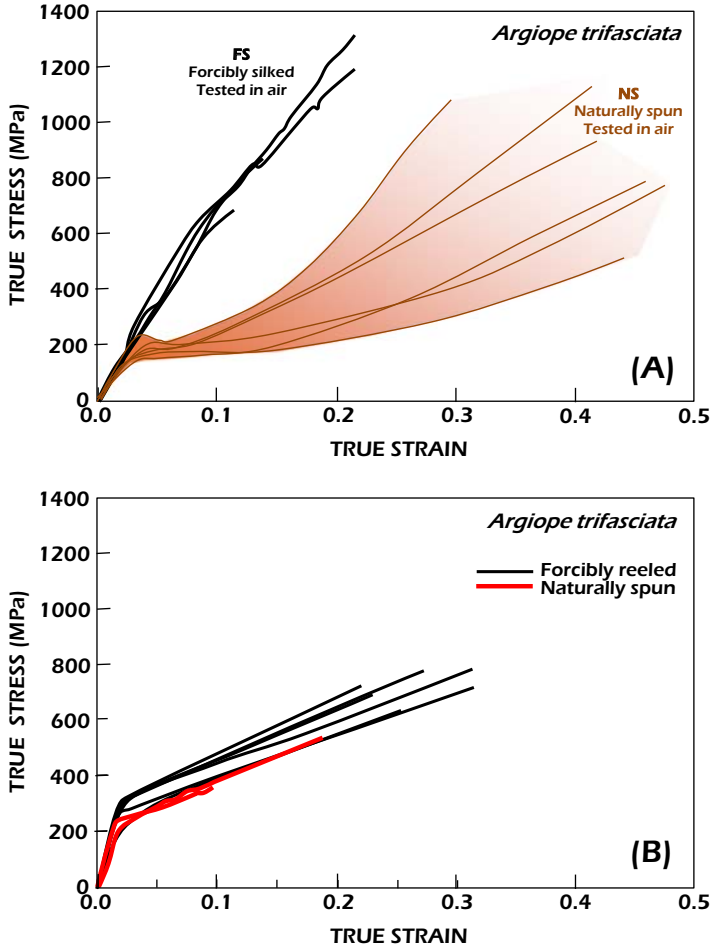

FIGURE 5.6 (A) Tensile properties of naturally spun (NS) and forcibly silked (FS) fibers of spider silks. (B) Tensile properties of NS and FS fibers from silkworm silks.

found in nature. These results suggest that the tensile behavior of MAS fibers can be modulated through the silking stress in a wide range that includes NS fibers.

In contrast to spiders, silkworm cocoons are an easy and straightforward way of obtaining substantial quantities (up to a 1000 m) of natural fibers with moderate variability [55], and constitute the primary source of this material. Single natural silkworm silk fibers are hard to obtain (usually from silkworms impeded to construct a cocoon) and silk reeled directly from the silkworm (forcibly silked) only permits receiving small portions of continuous fiber ($<3-4$ m).

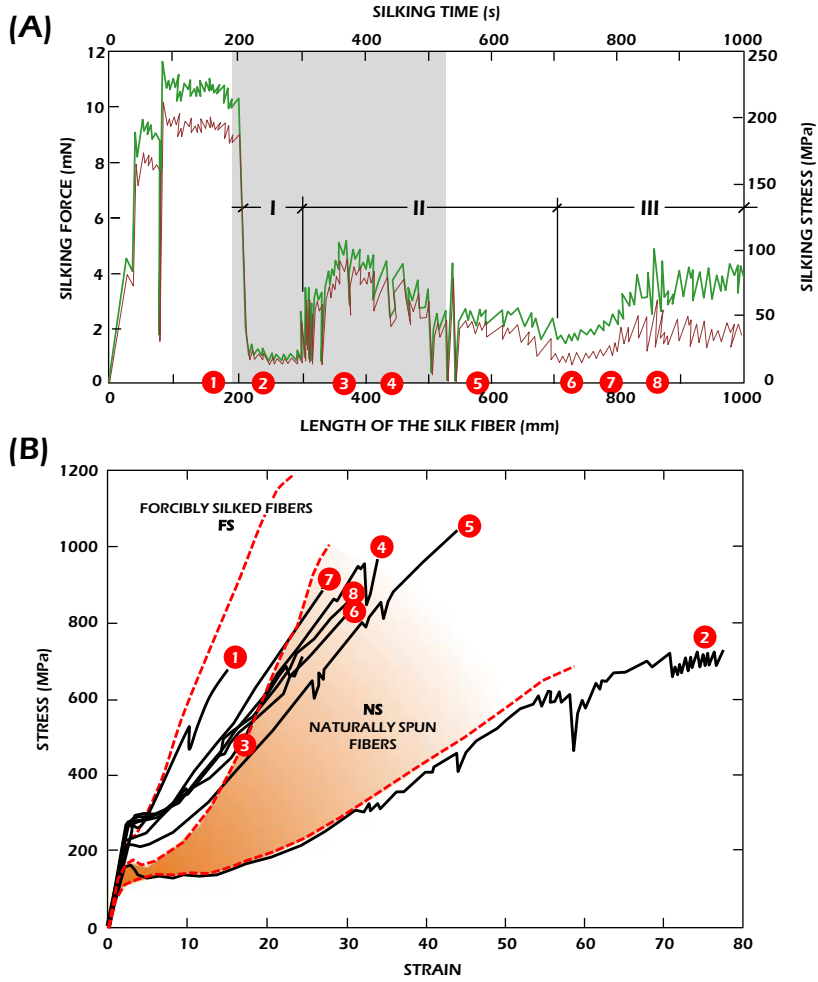

FIGURE 5.7 Spinning force and corresponding tensile properties of silk fibers from anesthetized spider [20]. Variation of the silking force and silking stress during the silking process at 1 mm/s of an anesthetized spider. The shadowed zone spans the period during which the spider was exposed to the CO_2 flow. The three regions—I, II, and III—correspond to the initial period of anesthesia (I), to an increase in the silking force followed by a smooth decrease (II), and finally region III begins from a minimum of the silking force. The samples whose tensile properties were measured are numbered from 1 to 8 [20].

While the properties of natural and FS silks are similar (Fig. 5.6B), silk from cocoons is altered during degumming, the process of removing the sericin coating (or silk gum) from the fibers. Degumming is ordinarily achieved by boiling native silkworm silk in water, sometimes in the presence of salt or detergents. Even in its mildest form (water only), it induces a decrease in

the initial elastic modulus and yield strength. It promotes a change in the shape of tensile curves, significantly increasing their variability [56].

Silkworm-silk fibers were obtained, mainly during the XIXth and the beginning of the XXth, by stretching the silkworm silk glands in a vinegar solution as an alternative procedure to natural spinning. This fiber—known as *silk gut fiber*—was widely used in fly fishing and, to a lesser extent, in surgical sutures.

Comparison of the tensile properties and microstructural organization of silkworm gut fibers with NS fibers, allows gaining a deeper insight into the mechanisms that lead to the formation of the fiber, as well as the relationship between microstructure and properties. For example, stress−strain curves of silkworm silk fibers and silk gut fibers are shown in Fig. 5.8A. Two kinds of silkworm silk fibers (one obtained by FS and another with subsequent degumming) and a silk gut fiber (produced by immersion in a 2% acetic acid solution for 2 min and subsequent stretching) are shown. Both are qualitatively similar, despite minor differences that can be traced back to variations in the crystalline phase between both fibers. The crystallinity of silkworm silk gut fibers is half of that measured for the natural fibers. Besides, the size of the β-nanocrystals in silkworm silk gut fibers is much smaller than that of native silk. However, despite the differences between the crystalline phases of both materials, there is a persistence in the number of β-pleated sheets that form the nanocrystals, suggesting that this might be a design principle in the formation of the fiber [57].

Silk gut fibers were also obtained by stretching spider guts from *Nephila inaurata* and *N. clavipes*. Spider silk gut fibers were achieved from the silk glands by immersion in a mild acid solution and subsequent stretching. The size of spider silk glands is much smaller than that of silkworms, making the stretching step more difficult. Glands used for *N. inaurata* were MAS glands [58] and for *N. clavipes* tubuliform silk glands [59].

Again, the comparison of silk gut fibers with their natural counterparts allows gaining new insights into the processing, microstructure, and properties of spider silks. In contrast to silkworm silk, major ampullate and tubuliform spider silk gut fibers are shown to be the same material as their natural counterparts. Tensile tests with mayor ampullate glands of both (natural and gut) fibers show the same behavior (Fig. 5.8B). Moreover, major ampullate spider silk gut fibers are endowed with the ability to supercontract and their properties concur with those of the natural material if both, silk gut fibers and native silk, are retrieved from the same species. The concurrence of the tensile behavior of tubuliform silk gut fibers and tubuliform native fibers of different species, points to the persistence of these silk fibers throughout evolution. The identification of spider silk gut fibers and native fibers, in this case, indicates that the processing instructions for forming the fibers from the protein solution are contained in the spidroins and are independent of the natural gland system [60].

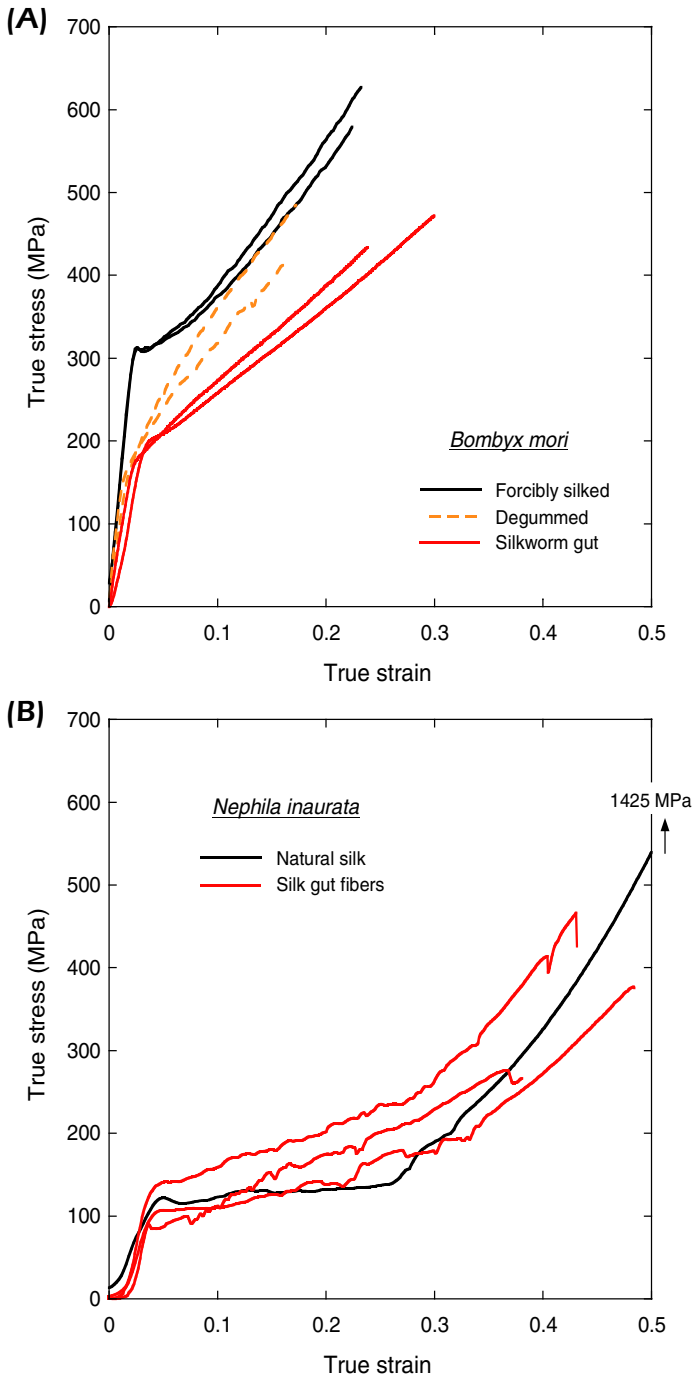

FIGURE 5.8 (A) Tensile tests with silkworm fibers (one obtained by forced silking and another after degumming) and silkworm gut fibers (produced by immersion in a 2% acetic acid solution for 2 mi and subsequent stretching). (B) Tensile tests with spider fibers from major ampullate glands. Comparison with natural fibers and silk gut fibers.

Silk gut fibers also offer a unique opportunity to monitor the early events leading to the formation of the fiber. In this regard, it was found [60] that the major microstructural change leading to the solid material is the appearance of β-pleated secondary structure at a strain of ∼100%. In addition, it is also found that the mechanical stresses required to complete the transition from the protein solution to the fibers are in the range of ∼1 MPa, which is a much smaller value than previous estimations suggested. Differences between these last values and those found from the analysis of natural spinning might arise from other forces that appear in the natural spinning process but are not directly involved in the liquid−solid transition. All these findings highlight the insights that can be gained from comparing silk guts and natural silk fibers.

5.3.3 Effect of water and temperature

Some silk fibers, particularly spider MAS, experience a (usually) large shrinkage when immersed in water and are free to contract, called supercontraction [23,28]. Supercontraction can account for up to half the initial length and can be quantified by the supercontraction (SC) index defined as:

$$\mathrm{SC} = (L_0 - L_{\mathrm{MS}})/L_0 \tag{5.5}$$

where L_0 is the initial fiber length and L_{MS} is the length of the supercontracted fiber once dried.

The SC index depends on the fiber type and condition; major ampullate NS fibers show a wider range of values of SC in correspondence to their variable tensile behavior: SC is between 0.3 and 0.5 for most species [46]. On the contrary, FS fibers are more homogeneous, with SC close to 0.5.

MAS fibers tested in water behave like elastomers [61] with an extremely low stiffness at small deformations that increases monotonically with deformation. In contrast, MAS fibers tested in air, either NS or FS or subjected to previous supercontraction and dried, behave like glassy polymers with a well-defined, nonzero, initial elastic modulus.

Humidity and temperature strongly influence the mechanical behavior of spider silk fibers; by increasing either or both, silk changes from a stiff, glassy polymer to a more compliant one, close to elastomers. This influence reflects in both the initial elastic modulus and the SC index, that display a sudden transition within the narrow range of values of humidity and temperature shown in Fig. 5.9 [62].

Silk fibers behave like a semicrystalline material with amorphous flexible chains strongly hydrogen bonded. For low enough temperatures and humidity, hydrogen bonds represent a significant contribution to the fiber's mechanical performance, showing a glassy behavior. The presence of water and/or high temperature disrupts the hydrogen bond network, promoting the

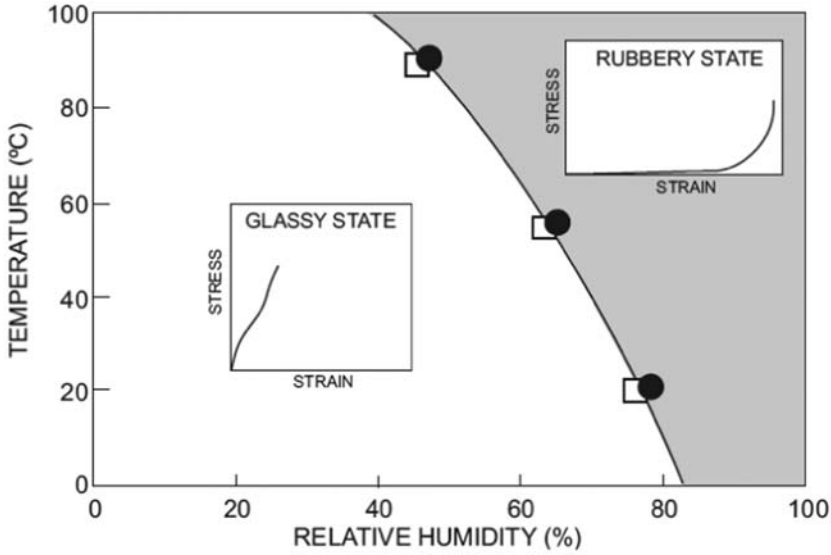

FIGURE 5.9 Transition from the glassy to the rubbery state as a function of relative humidity and temperature. Transition values of supercontraction index (open squares) and initial elastic modulus (full circles) are indicated [62].

rubbery behavior and, thus, the supercontraction phenomenon is explained by the plasticizing effect of water [62].

An outstanding feature of MA spider silks is the fact that the properties of supercontracted fibers are invariant and independent of both the previous loading history and the collection procedure (natural or forced silked) [63]. The silk state after maximum supercontraction (Ms)—which can be regarded as a type of annealing—can be considered a mechanical "ground state" from which silk fibers can be tuned with predictable and reproducible features.

This is illustrated in Fig. 5.10, where it is shown how—independently of its origin—the stress−strain curves of supercontracted fibers merge into a unique behavior. A practical consequence is that, unlike other materials, spider silk can recover from inelastic deformations by simple immersion in water and subsequent drying.

Most interestingly, the existence of the Ms ground state opens the possibility of tuning the properties of MAS fibers in a predictable and reproducible way using the wet stretching process, summarized in Fig. 5.11 [45].

In this process, a fiber is allowed to freely contract in water up to the maximum supercontracted length L_{MS}. It is then stretched to the desired length L_A, and dried overnight with its ends clamped. The stresses built up in the fiber during drying are relaxed by unloading the fiber to the final length, L_C (see Fig. 5.11A), at the last step of the process.

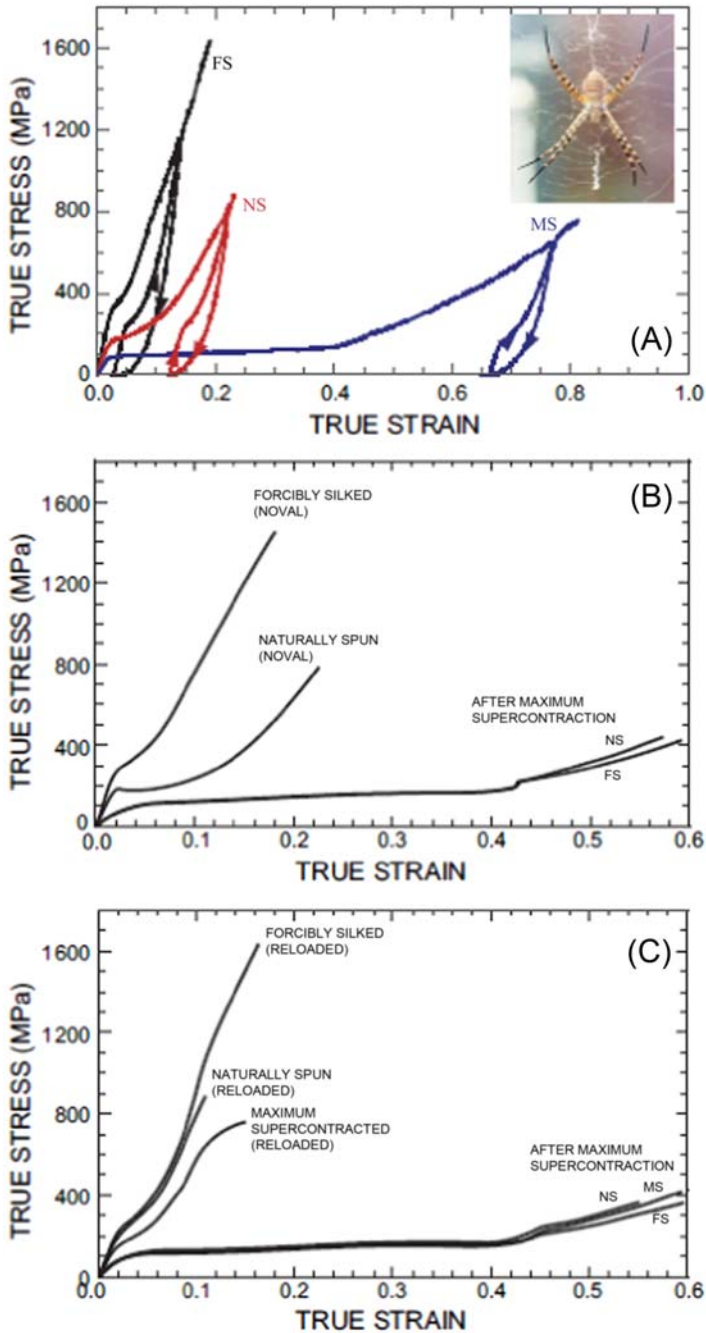

FIGURE 5.10 (A) Stress−strain curves of forcibly silked (FS), naturally spun (NS), and maximum supercontracted (Ms) fibers: noval curves and curves after unloading and reloading cycle (major ampullate silk from *A. trifasciata*, see inset). (B) Stress−strain curves of noval FS and NS fibers before and after Ms. (C) Stress−strain curves of previously deformed FS, NS, and Ms fibers before and after Ms [63].

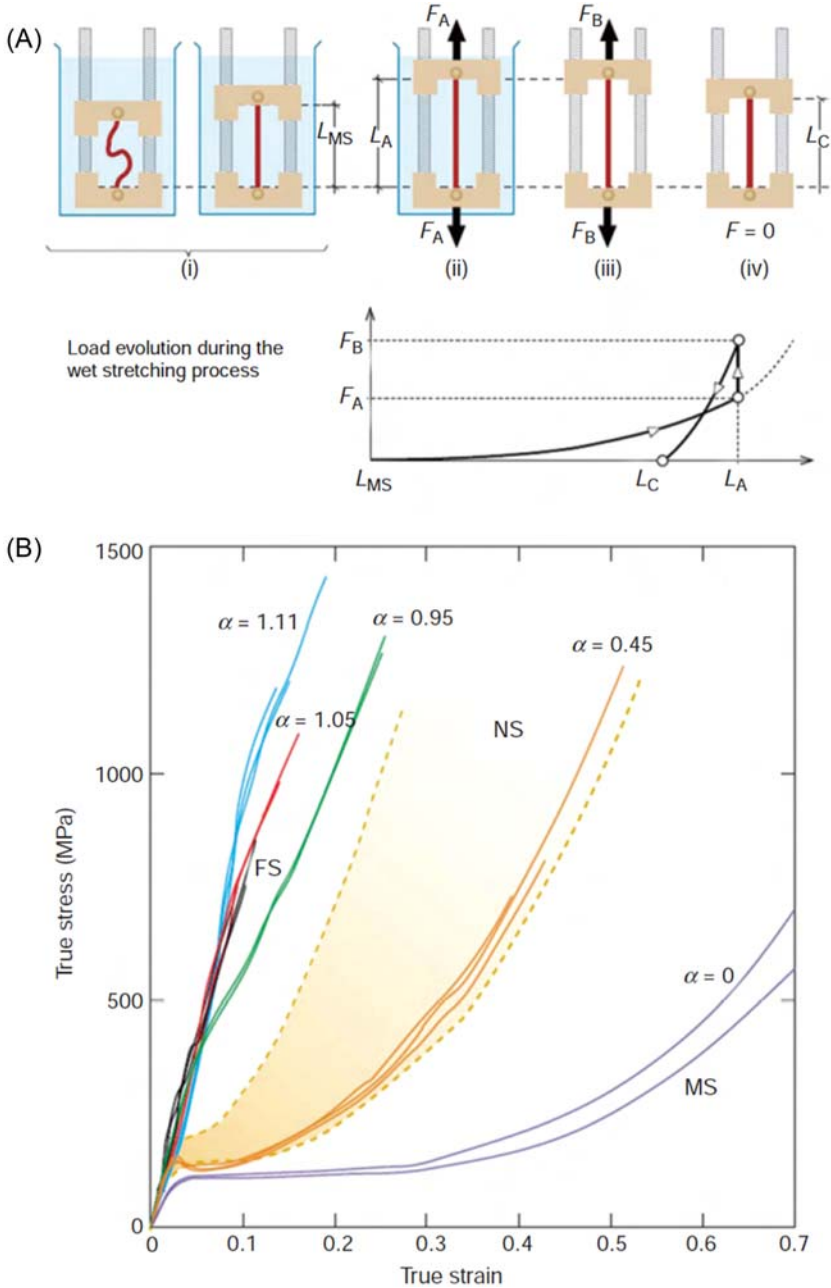

FIGURE 5.11 (A) Wet stretching procedure: (i) supercontraction in water; (ii) stretching in water; (iii) drying; (iv) final unloading. *LMS*, stabilization length; *LC*, final length; *LA*, desired length. (B) Stress–strain curves obtained with the wet stretching procedure, using different values of the alignment parameter α. Note that for α close to 1.0, typically forced silked (FS) fibers (also shown) are reproduced. The span of natural silked (NS) fibers ranges between $\alpha = 0.45$ and $\alpha = 0.90$. The ground state (Ms) corresponds to $\alpha = 0$ [45].

The alignment parameter α, defined as:

$$\alpha = L_C/L_{MS} - 1$$

quantifies the stretching of the fiber from the ground state (MS), where it takes a value $\alpha = 0$.

Fig. 5.11B shows the tensile curves of fibers mechanically tuned by the wet stretching procedure with alignment parameters ranging from $\alpha = 0$ to $\alpha = 1.1$. FS fibers are reproduced with $\alpha = 1.11$, while NS fibers are replicated with values of the alignment parameter between $\alpha = 0.45$ and $\alpha = 0.90$.

The results above highlight the importance of the existence of the ground state, a property that underlies the shrinkage of the fibers in humid environments (supercontraction), their recovery after irreversible stretching and the tuning of the mechanical properties of MAS.

Wet stretching has shown that the mechanical behavior of all *Entelegynae* MAS fibers, under any conditions, is described from the maximum supercontracted state by the *aligment parameter* α that connects the sequential action of three deformation micromechanisms during stretching: stressing of protein−protein hydrogen bonds, rotation of the β-nanocrystals concerning the macroscopic axis of the fiber, and growth of the crystalline fraction [64]. Conservation of these traits for over 230 million years indicates the optimal design of the material and gives valuable clues to produce biomimetic counterparts based on major ampullate spider silk.

Tensile properties of spider major ampullate gland silks vary among species, but this variation is confined to evolutionary shifts along a single universal performance trajectory. This reveals an underlying design principle maintained across significant spider ecology and silk chemistry changes. The persistence of this design principle becomes apparent after the material properties are defined relative to the true alignment parameter, which describes the orientation and stretching of the protein chains in the silk fiber. Moreover, a new procedure—S^3I, based on the generalized alignment α^* parameter—allows the classification of the tensile properties exhibited by major ampullate gland silks spun by *Entelegynae* spiders [65,66]. S^3I was launched under the assumption that systematic knowledge of the values of the α^* (alpha-star) parameter for as many species as possible will improve our current understanding of major ampullate spider silk.

Elucidating how the original design evolved over the 400-million-year history of spider silk and identifying the fundamental relationships between microstructural details and performance have proven complex tasks. The analysis of *maximum supercontracted* spider silk fibers using XRD shows a complex picture of silk evolution where some key microstructural features are conserved phylogenetically. In contrast, others show substantial variation among closely related species [67]. These results help unravel the microstructural features, which must be copied to produce the next generation of biomimetic silk fibers.

The exceptional recovery properties and mechanical tunability can be imparted to regenerated silkworm *B. mori* silk fibers by appropriate processing [10]. Regenerated fibers showed properties not displayed by natural silkworm silk (ability to recover from irreversible deformation, modifiable tensile behavior), which had been considered exclusive to natural spider silk. These results prove that processing plays a role comparable to composition in the final properties of silk fibers, even prompting the emergence of new properties to recover the outstanding properties of the natural materials.

5.4 Relationship between structure and properties

The hierarchical structure of spider silk has been analyzed with simulations on several scales, from the repeat unit of a set of dragline silk protein strands in atomistic resolution to mesoscale models of fibrils and, eventually, to the whole spider web. These studies address the relationship between structure and properties and how material phenomena at the molecular scale affect material properties and, ultimately, the function of the spider web. Reviews by Buehler and collaborators [68,69] provide a good insight into this topic.

5.4.1 Microscopic models

All silk fibers are shown to contain two phases: crystalline and noncrystalline, that yield what is described as a semicrystalline microstructure.

In both silks, silkworms and spiders, a nanocrystalline phase appears that results from the piling up of β-sheets. The β-sheets of spider silk are formed from the polyalanine ($-A_n-$) motifs, while those of *B. mori* silkworm silk corresponds to the −GAGAGS− motifs. Despite using such powerful microstructural characterization techniques as NMR, the present knowledge on silks' noncrystalline phase (sometimes referred to as the amorphous phase) is much scarcer.

The microstructural characterization of the crystalline phase of spider silk took advantage of using synchrotron sources for the characterization of single fibers. In particular, the combination of single-fiber XRD and the possibility of harnessing the variability of the fibers through supercontraction allowed a thorough comparison of the crystalline phases of a set of representatives from the *Entelegynae* suborder [67]. All diffraction patterns were taken from individual fibers of the related species after being subjected to Ms. The analysis of the diffraction patterns showed that all analysed species of the *Entelegynae* suborder presented a typical unit cell, which corresponds to the β(3) group of the classification proposed by [70].

In addition to identifying the unit cell of a crystalline phase, XRD also allows extracting information on three highly relevant microstructural features of silk fibers: the size of the nanocrystals, the orientation of the nanocrystals concerning the macroscopic axis of the fiber, and the ratio between

crystalline and amorphous phases, usually measured as the percentage of crystalline phase or crystallinity. Thus, establishing the similarities and differences in these microstructural features among the fibers spun by different species would be a valuable hint to determine their likely influence on the variability observed among the studied species.

The analysis of the size of the nanocrystals did not show remarkable variations between the fibers and consequently, this microstructural feature was not considered relevant in causing the observed differences. In contrast, significant differences were observed when analyzing the nanocrystals' orientation concerning the fiber's macroscopic axis. A similar situation was found to apply when comparing the values of crystallinity [71].

The mechanical properties, particularly high strength and elasticity, of spider and silkworm silks are related to silk microstructure, which depends on the amino acid sequence and their singular microstructures. Most of the experimental work has been done by tensile testing of silk fibers, as discussed in Section 5.3, stiffness, strength, deformation, and toughness can be measured from a tensile test, and testing under different humidity and temperature can provide exciting results about the influence of water and temperature on the microstructure.

Silk microstructure is conditioned by the role of amino acid motives and the part of processing, as discussed in Section 5.2. The highly conserved poly-Ala repeats provide stiff, orderly cross-linking domains embedded in a semiamorphous matrix of less ordered Gly-rich repeat units. During the processing of silk, the flow in the spinning duct leads to stretching and aligning proteins. Both processes influence the microstructure, particularly secondary structures of proteins, and are relevant for understanding the mechanical behavior of silks.

Computations ab initio of the mechanical behavior of silk fibers are still in their infancy due to the complexity of their large polymeric chains. Even so, two models deserve being briefly pointed out: an atomistic one [72] and a molecular one [30,73].

Keten and Buehler have provided an atomistic model based on a bottom-up computational approach using replica exchange molecular dynamics [74]. This model supports the observation of β-sheet structures of poly-Ala domains, hydrogen-bonded 3_{10}-helix structures of semiextended GGX (i.e., Gly−Gly−X [with X = Leu, Gln, or Tyr]) domains, and the lack of α-helical conformations. These findings are validated against experimental results. Also, the model predicted an increase in the fractions of the aligned β-sheets for large deformations of the silk fiber [75]. The model sets the stage for atomistic studies on silk domains that will contribute toward an improved understanding of the source of the strength and toughness of the silks.

Termonia [30,73] developed a molecular silk model, sometimes called the double lattice model, which bypasses details of the deformation on an

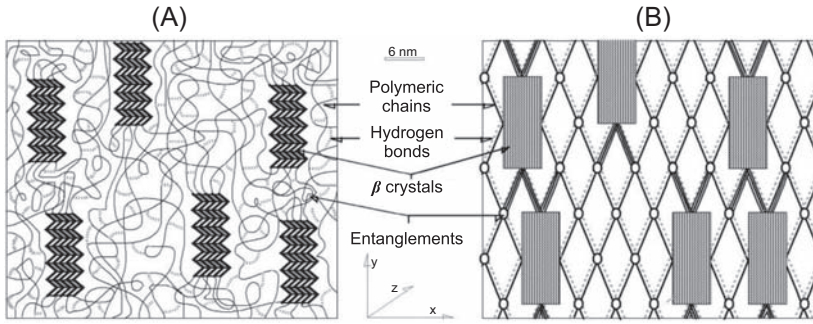

FIGURE 5.12 Molecular model for spider dragline. (A) System of amorphous and crystalline chains. For straightforward representation, the figure is for a 15% volume fraction of β-pleated sheets; (B) more schematic representation in which the details of the amorphous chains have been omitted and only end-to-end segments are shown. Individual hydrogen bonds have been replaced by "overall" bonds (dotted lines) connecting every entanglement to the neighbors. The three-line segments indicate the high modulus layer in the amorphous phase [30].

atomistic scale and focuses instead on a length scale of the order of the distance between entanglements. Silk fibers were modeled as a semicrystalline material made of amorphous flexible chains reinforced by crystallites, as depicted in Fig. 5.12. Initial lattice parameters such as molecular weight, the density of entanglements, crystalline fraction, etc., were fixed from experimental data. Fibers are modeled as a network where knots are the nanocrystallites or the entanglements and threads the amorphous chains or hydrogen bonds connecting every entanglement to their neighbors.

The lattice deformation was performed in a succession of tiny length increments. After each strain increment and upon complete relaxation of all lattice sites, individual bonds and entanglement points were visited at random by a Monte-Carlo lottery and four processes were allowed to occur:

- breaking of the hydrogen bonds;
- stretching of the chains in the amorphous regions;
- breaking of the chain strands in the amorphous regions; and
- network relaxation.

After the network of entanglements had been fully relaxed toward mechanical equilibrium, an additional elongation increment was applied to the network. The four processes described above restarted for another time interval. This was repeated and continued until the network failed.

This model made qualitative and quantitative predictions of stress−strain curves, as shown in Fig. 5.13A. Using reasonable initial data (see [30]) the model predicted at minor strains—under 0.002—a linear curve with modulus $E = 10$ GPa, in agreement with experimental observation [28,50,77]. At about 0.02 strain, the hydrogen bonds between chains in the amorphous region started to break, forming a yield point at which the stress−strain

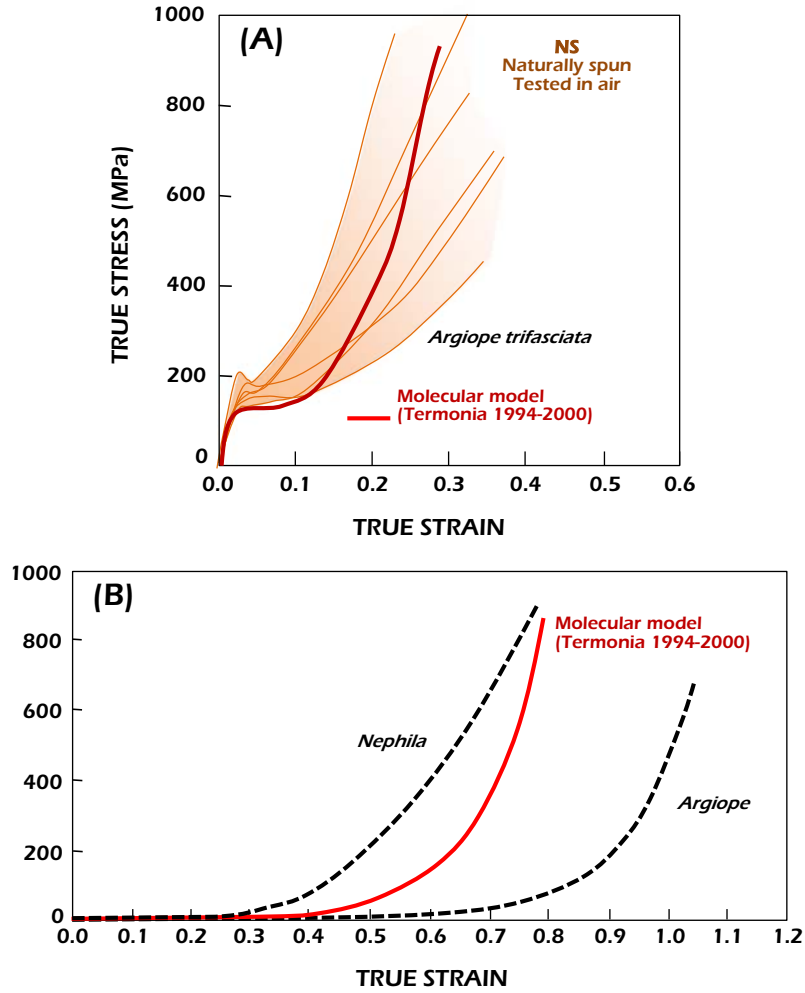

FIGURE 5.13 (A) Calculated and experimental stress–strain curves for spider dragline silk fibers [32]. (B) Calculated and experimental stress–strain curves for spider dragline silk fibers (immersed in water and then strained at a rate of 1.42/min) [76].

curve reached a plateau. At 0.1 strain and higher, the hydrogen bond-breaking process was almost complete, and the stress resumed its increase with strain. Fracture at strains circa 0.3 occurred in agreement with most experimental results.

The model also reproduced the effect of water in the stress–strain curves. The model assumed that the only impact of water on the fiber was to prevent the formation of hydrogen bonds between chains in the amorphous phase. Upon stretching the network, now free of hydrogen bonds in the amorphous

phase, the stress−strain curve exhibited a rubber-like behavior (Fig. 5.13B). Also represented in this figure are typical experimental curves for wet draglines from two spiders [46].

5.4.2 Macroscopic models

Macroscopic models are based on the mechanics of continuous media and use constitutive equations that capture the main microstructural features. Other macroscopic models are based on the mean field theory for polymers in terms of chemical composition and degree of order in the polymer structure. A brief description of both models is summarized.

The model by Planas, Elices, and Guinea, based on the mechanics of continuous media [78], regards the silk fiber as a fiber-reinforced material made with sets of microfibrils dispersed into a deformable matrix. It is also assumed that no force is transmitted through the matrix in the composite material (i.e., that the matrix is perfectly deformable and stresses build up in the microfibrils only as a consequence of deformation). To make the analysis simple, the equivalent continuum macroscopic model is introduced by forcing it to give the same mechanical work as the fiber-reinforced material (i.e., spider silk fibers) under any arbitrary motion. This condition had to be complemented by the relationship between the nominal stress and strain within the microfibrils [78]. For this relationship, a simple model was postulated, capturing the well-known behavior of spider silks, a nonlinear spring representing the stretching and orientation of molecular chains in the rubbery state (i.e., with the network of hydrogen bonds deactivated), in parallel with a skidding block with a linear spring to account for the breaking of hydrogen bonds and molecular slippage when the fiber was under the glass transition.

Fig. 5.14 shows the experimental results of tensile testing performed in air of spider silk fibers (MA) with three different degrees of molecular alignment identified by the alignment parameter α, obtained as described in Section 5.3 [45]. In the same figure, the results of numerical computations are determined using the macroscopic model for the three kinds of fibers. Each type of fiber is characterized by the orientation index β [78], which can be interpreted as the ratio between the projected length of the microfibrils along the fiber axis and their total length at a given instance. A random orientation of microfibrils gives $\beta = 0.5$, whereas $\beta = 1$ stands for all the microfibrils parallel to the fiber axis. As shown in Fig. 5.14, the agreement between experiments and simulation is remarkable, especially considering that the numerical modeling reproduces the experimental procedure step by step. The proposed model follows the large deformation of MAS fibers and adequately captures their alignment process, easily incorporating the main operative microstructural mechanisms.

The *mean field theory for polymers* has been used to predict structure−property relationships for the mechanical properties of silk fibers in terms of

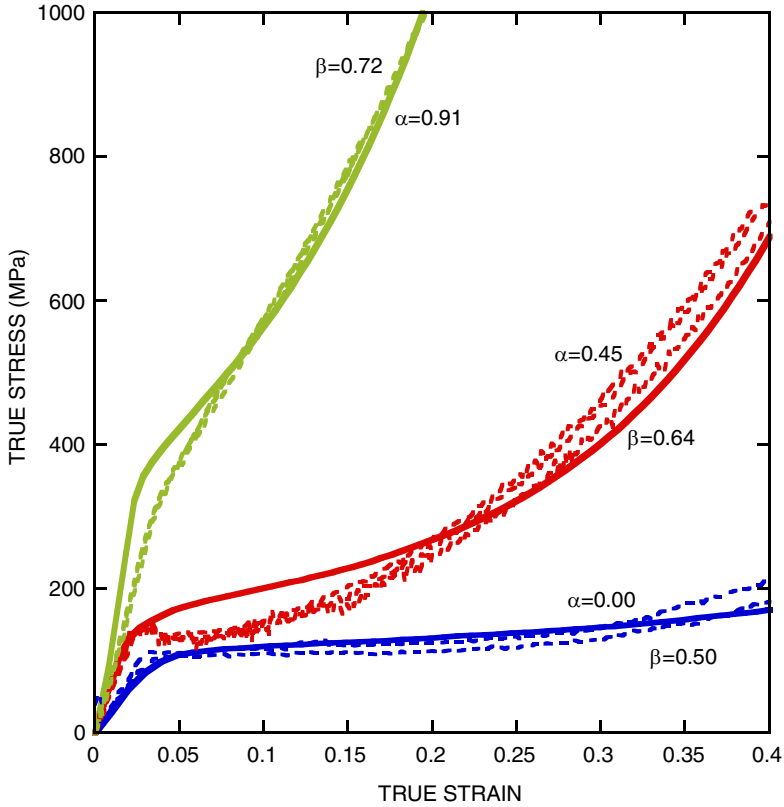

FIGURE 5.14 Calculated and experimental stress–strain curves for spider dragline fibers. Model results are labeled by the orientation index β. Experimental data are identified by the alignment parameter α.

chemical composition and morphological structure [79]. Silk fibers are modeled as a composite material with ordered and disordered phases: the more rigid domains are dispersed at a nanometer scale within the less rigid amorphous phase. The nanoscale morphology allows the two phases to share energy at the molecular level and behave in bulk as a homogeneous material [80].

The analysis uses a mean-field modeling method called group interaction modeling, developed by Porter and Vollrath [81]. The chemical composition of silk proteins is embodied in the model parameters of poly-Ala, whose morphology is quantified by the single variable parameter of the fraction of ordered phase (similar to the alignment parameter α [45]). The mechanical properties of silk fibers are derived from the ordered fraction. This information helps draw simplified stress–strain curves, whose envelope agrees with experimental observations, as shown in Fig. 5.15.

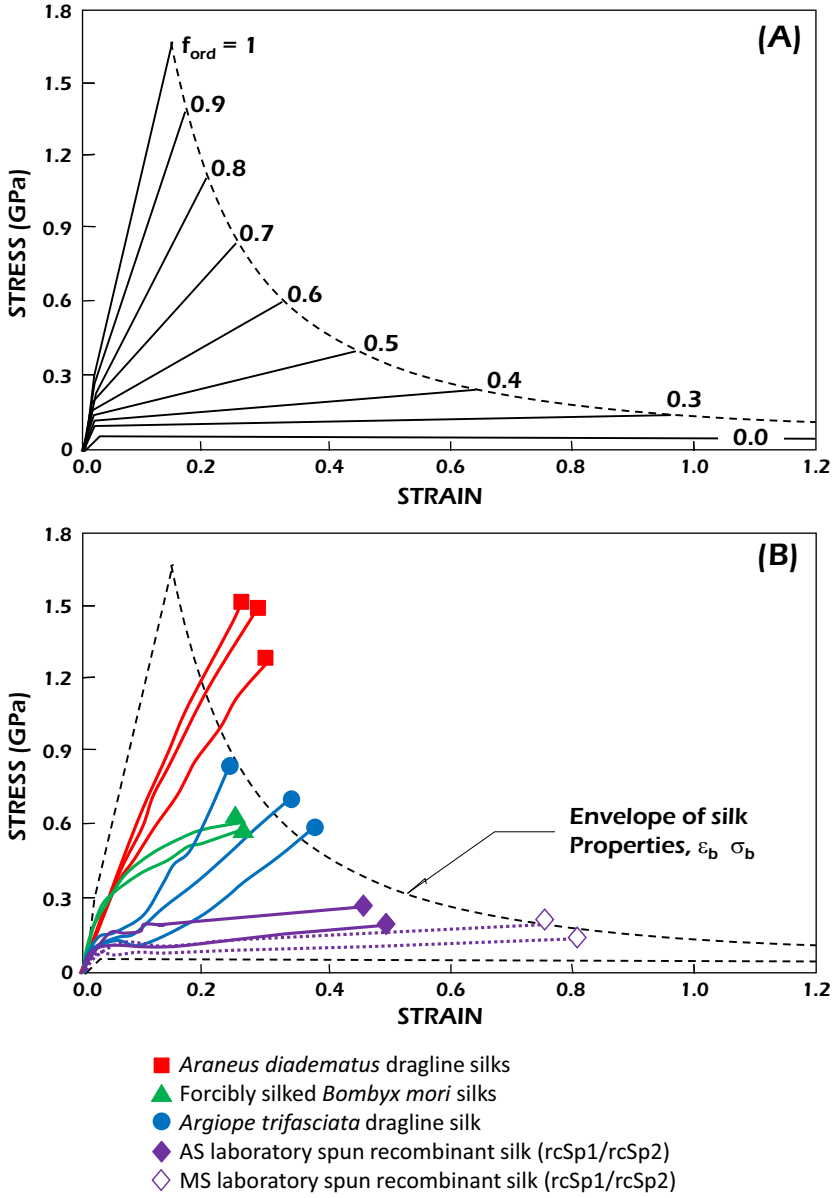

FIGURE 5.15 (A) Simplified stress–strain curves, according to Porter's model [79] for different degrees of order (ford, from 0 to 1). (B) Envelope of simplified stress–strain curves and experimental results from the authors [44,46,76]. *AS*, as-spun; *Ms*, maximum supercontracted.

5.5 Biomimetic approaches

Biomimetics intends to develop and organize the knowledge required to reproduce the particular properties of biological materials in their artificial counterparts [82]. In the field of silk fibers, the aim is to understand, replicate, and improve (if possible) the properties of natural silks by mimicking their composition, microstructure, and processing. Ideally, the objective is to gain the ability to spin the fibers from an appropriate dope and to tune them within the range of accessible properties described in the previous sections.

There are four different approaches to producing the dope feedstock from which silk can be spun [83]: (1) the obtaining of the dope from the silk gland of silkworms or spiders; (2) the regenerating route in which the solution of silk proteins is obtained by dissolving the fibers and then concentrating them by dialysis; (3) the genetic engineering techniques, that is, using modified organisms to express transgenic proteins with a sequence inspired by the natural silks, then purifying the proteins; and (4) the synthetic way. Only the regenerating and genetic routes have been extensively used until now, and they are outlined in the following two subsections.

Regarding the spinning techniques, although there are some reports of microfluidic devices that allow the modification of the pH of the dope during spinning [84,85], most processes are based on the wet-spinning technique [86], which requires the formation of a spinnable dope that solidifies into a fiber in a coagulating bath. Additionally, a second step of stretching the fibers is commonly used. In some works, it was carried out in the water or an atmosphere of water vapor.

5.5.1 Regenerated silkworm silk

The relative ease with which silkworm (*B. mori*) silk fibroin can be obtained in comparison with spider silk spidroins has stimulated the development of artificial spinning systems to produce regenerated silkworm silk fibroin fibers. In addition, this route is exciting for the development of biomimetics since the study of regenerated fibers leaves one basic unknown (processing), as the other (composition) is the same as in the natural material. Regenerated (or reconstituted) *B. mori* silk-dope solutions are made from the cocoons built by the silkworms, dissolved in strong chaotropic (hydrogen-bond disrupting) solvents prepared from inorganic or organic salts, concentrated acids, or fluorinated organic compounds. Among them, LiBr is often used. Once the silk proteins are dissolved, the solutions are dialyzed to remove the chaotropic molecules.

The procedures for spinning regenerated fibers differ essentially in the composition of the initial dope and, to a lesser extent, in the design of the coagulation bath. Thus, several dope compositions that yield spinnable solutions have been reported, such as saturated ammonium sulfate solution [87],

concentrated ortho-phosphoric acid [88], concentrated aqueous solution [89,90], hexafluoroisopropanol (HFIP) [91,92], hexafluoroacetone hydrate [93], formic acid [94,95], ionic liquids [96,97], and N-methyl morpholine oxide (NMMO) [98].

The spinning of regenerated silkworm silk fibers has proved highly challenging, as reflected by the poor tensile properties reported by most studies [89,94,98,99]. It was only after setting up subsequent changes in the basic wet-spinning process, primarily related to the introduction of modified postspinning drawing processes that the first reports of the production of high-performance regenerated silkworm silk fibroin fibers with properties comparable to those of the natural material were found [10,100–102].

One example of a successful way to obtain fibers with such properties is to utilize a final step of water immersion postspinning drawing (IPSD) [10,34]. This process, using fibroin in NMMO aqueous solution and methanol as a coagulant, is sketched in Fig. 5.16. The possible range of the values of the drawing ratio during the coagulation (Dr_1) and the ratio during the immersion in water (Dr_2) is also represented.

It was found for this material that low values of the two ratios yield brittle fibers. However, the water IPSD step allowed ductile and stronger fibers to be obtained, which were endowed with two of the distinctive properties of spider silk fibers: *supercontraction* and *recovery* (see Fig. 5.17). Also, the microstructural analysis showed that the crystallinity in these fibers ($\sim$20%) was similar to that of the spider silk fibers ($\sim$15%) and clearly lower than the silkworm silk fibers ($\sim$60%). These properties can be explained by a high mobility of the protein chains during water immersion, combined with the stresses generated during postspinning drawing, yielding an improved arrangement of the chains, and a reduction in the density of entanglements in the amorphous region. Further, in contrast to regenerated fibers subjected to postspinning drawing in air, water immersion provided completely homogeneous drawn fibers, as observed using AFM [104].

The emergence of supercontraction in regenerated silkworm (*B. mori*) silk fibers have been assessed through an experimental approach that combines the spinning of regenerated fibers and their characterization by ^{13}C solid-state NMR [105]. Both supercontracting and nonsupercontracting regenerated fibers were produced using the straining flow spinning (SFS) technique from ^{13}C-labeled cocoons. The short-range microstructure of the fibers is assessed through ^{13}C cross-polarization magic angle spinning in air and ^{13}C dipolar decoupled magic angle spinning in water, and the main microstructural features are identified and quantified. The mechanical properties of the regenerated fibers and their microstructures were compared with those of natural silkworm silk. The combined analysis highlights two possible key elements as responsible for the emergence of supercontraction: (1) the existence of an upper and a lower limit of the amorphous phase compatible with supercontraction; and (2) the existence of two ordered phases,

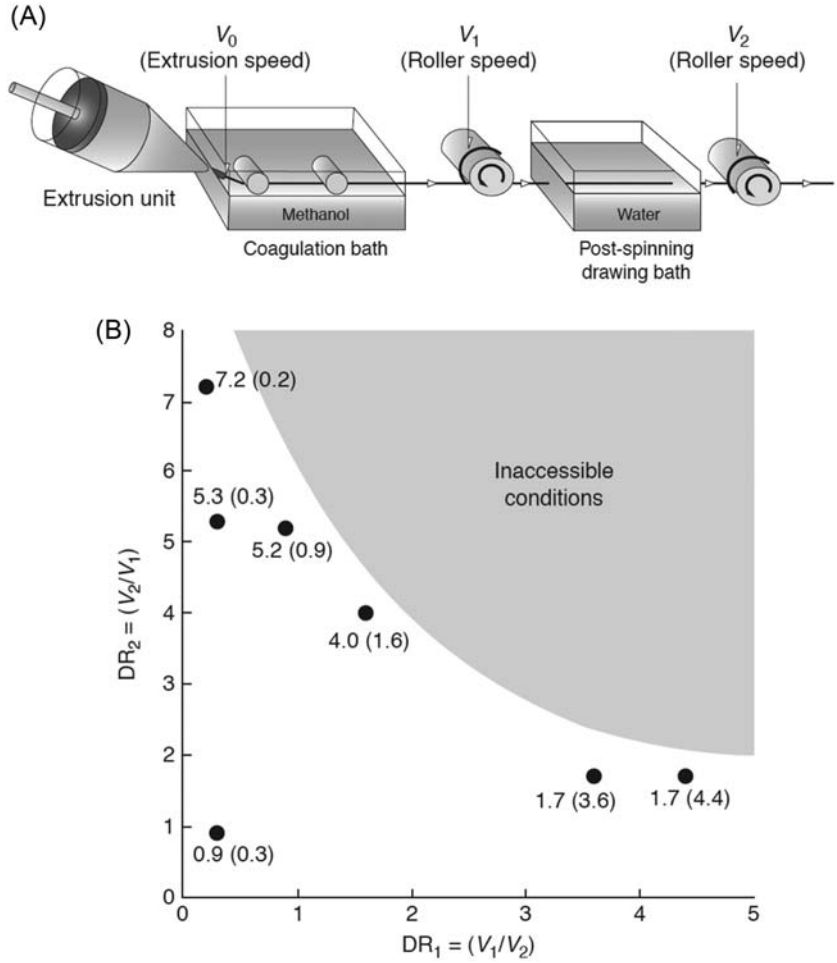

FIGURE 5.16 (A) Sketch of the spinning process of regenerated silkworm silk fibers. (B) The graph shows the range of possible combinations of ratios during the spinning process [103].

β-sheet A and B, which correspond to different packing arrangements of the protein chains.

In addition to these conventional spinning techniques, the increased knowledge of the natural spinning process has led to the development of new biomimetic approaches. In this context, SFS derives from flow focusing and wet-spinning technologies, and its principal characteristic is that the physicochemical environment of the dope, as well as the mechanical stresses to which the fibroins are exposed, are controlled by the interaction of the dope with a jet of focusing fluid [106,107].

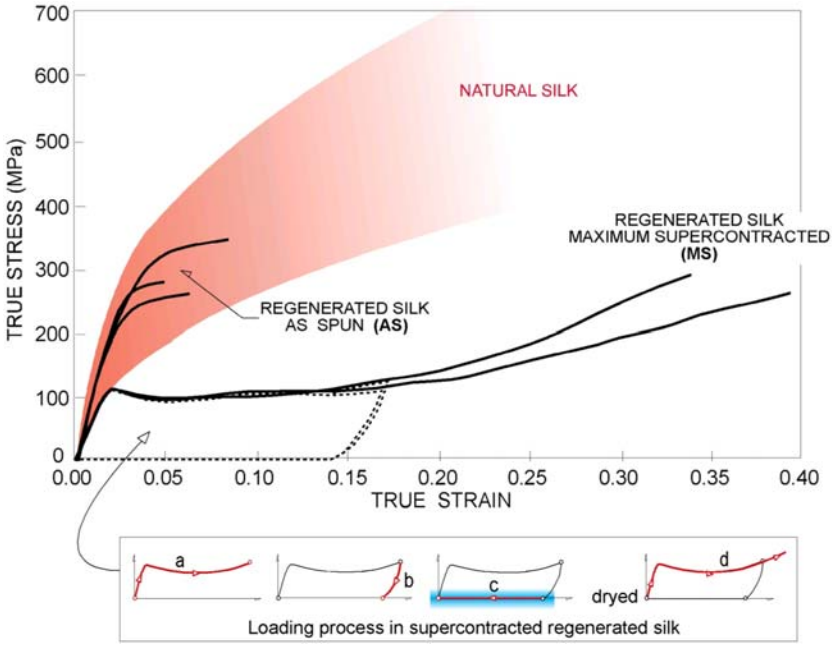

FIGURE 5.17 Stress–strain curves of IPSD fibers in the as-spun condition (AS) and after maximum supercontraction (Ms). Recovery process: (A and B) loading and unloading test of Ms fiber; (C) water immersion; and (D) new loading process.

In this regard, the versatility of SFS is the result of a large number of geometrical and hydrodynamic parameters [108], as well as the chemistries of the coagulants that can be employed [109]. Thus, compared with most wet-spinning and electrospinning approaches, the inclusion of geometrical and hydrodynamic processing parameters as an integral part of the technique allows spinning under a much more comprehensive range of chemistries. In particular, remarkable results were obtained while restricted only to aqueous-based and environmentally friendly chemistries [110,111]. The production of high-performance and biocompatible silk fibers opens up a wide range of novel applications in biomaterials, including sutures, prostheses for tendons and ligaments, and scaffolds in tissue engineering.

5.5.2 Genetically engineered spider silk

Genetic engineering techniques allow cloning proteins to mimic the primary structure of natural spider silks, with a molecular weight significantly lower than that observed in natural proteins [112]. This limitation requires establishing an initial hypothesis on (1) which parts of the natural protein are essential for their performance and (2) how they should be organized

[85,113,114] in order to decide the sequence. Some works have focused on the sequence elements that contribute to the formation of the fibers during the spinning process, particularly the nonrepetitive regions at the N- and C-termini [18,115]. The expression of these analogs has proceeded successfully in several different organisms, such as bacteria [116,117], yeasts [118,119], plants [120], and animal cells [112–114]. In some cases, reports on fibers produced from genetically engineered proteins that may surpass the properties of the natural material may be found [121]. Genetically engineered silks have been studied as biomaterials in tissue engineering [122]. Scheibel [123] and Chung et al. [124] have reviewed the production, processing, and applications of recombinant spider silk.

The first attempt to obtain artificial fibers from a solution of recombinant proteins was reported by DuPont [125] using HFIP as a solvent and spinning through a stainless-steel spinneret into a coagulating bath of isopropanol. Nexia [112] produced fibers with good tensile properties using transgenic goats expressing spidroin-like proteins (diadematus fibroin 3 [ADF-3], MW = 60 kDa) in their mammalian cells, which were then dissolved in phosphate-buffered saline aqueous solution and a methanol–water coagulating bath. Later attempts have tried to incorporate part of the complexity observed in the silk glands of arthropods through the inclusion of processes such as salting out, pH drop, and elongational flow during the spinning process [85] or with the use of microfluidic devices [84].

In the procedure initially developed by Nexia, the bioinspired silk proteins are obtained in the milk, from which they are purified. Given the absence of other toxic molecules, it appears as an up-and-coming source for the silk proteins to be used in the biomedical field. This method allowed collection of two proteins inspired by the two spidroins (MaSp1, MaSp2) of the species *N. clavipes*, which were labeled rcSp1 and rcSp2, respectively [76]. As explained in the previous sections, a distinctive characteristic of the spidroin MaSp2 is the high content of the amino acid proline, which has been linked with the supercontraction phenomenon [126,127].

Fibers composed of the proteins rcSp1 and rcSp2 were obtained using HIFP as solvent and isopropanol as coagulant [76]. Interestingly, a few differences were found between fibers with different relative contents rcSp1 and rcSp2, and both showed the supercontraction phenomenon, demonstrating that proline is not a requisite. In addition, these bioinspired fibers were indistinguishable from natural spider silk in terms of their tensile behavior except at substantial deformations (see Fig. 5.18), indicating that the microstructural organization is significantly maintained in the bioinspired fibers.

The results obtained with bioinspired fibers provide a better understanding of the key features underlying the excellent mechanical performance and properties of natural silks, and it is now known that many initial prerequisites on the composition of the recombinant fibers can be significantly relaxed. At the same time, processing is appointed a leading role. In this regard, it is

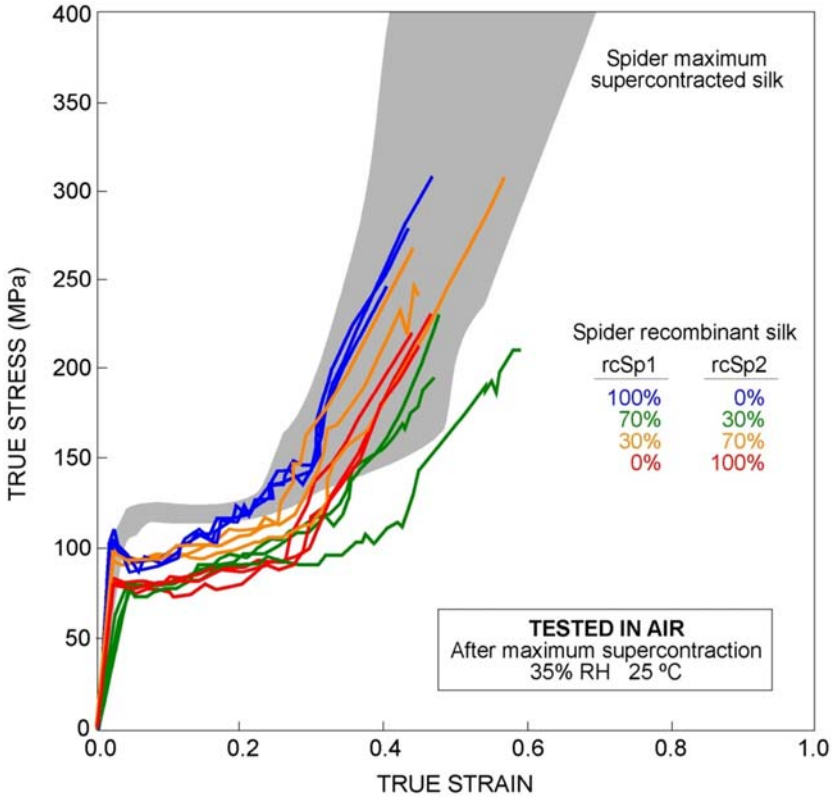

FIGURE 5.18 True stress–true strain curves of maximum supercontracted bioinspired fibers of four compositions based on the recombinant proteins rcSp1 and rcSp2 (mimicking, respectively, the primary structure of the protein MaSp1 and MaSp2 in the major ampullate silk of the spider *N. clavipes*, see text) [76]. Fibers tested in the air after maximum supercontraction, 35% RH, 25°C. The shaded area corresponds to the range of tensile properties of maximum supercontracted fibers exhibited by spiders of the *Araneoidea* lineage.

expected that future advances in spider silk-like, bioinspired fibers will provide valuable insights to foster the use of regenerated silks obtained from cocoons, a wide and versatile source of scaffold biomaterials.

5.6 Some medical applications

In spite of a long—albeit limited—application of silks for biomedical purposes [128,129], nowadays silk-based medical products available in routine clinical use are limited to a silk surgical mesh (SERI Surgical Scaffold), silk sutures, and silk clothing to treat dermatological diseases. All these products are produced with *B. mori* natural fibers [130].

Silkworm silk fibroin, in its native or regenerated forms, has features suitable for applications in tissue engineering scaffolds. To quote some, it provides templates for tissue regeneration in skin, bone, cartilage, tendon, or nerve [131−135].

In particular, concerning nerve regeneration, silk fibroin appears to be a promising biomaterial. Brain damage stands as the leading cause of neurological dysfunction in humans. Effective therapies to promote substantial recovery after brain injury are currently not available. Silk fibroin meets most of the standards of a biomaterial suitable for this purpose. Compared with other biomaterials, such as collagen or polylactic acid, silk induces a lower inflammatory response [136]. Although this biomaterial has never been used in preclinical models of brain repair, silk fibroin composites have been employed in the regeneration of peripheral nerves in rats [137].

Silk fibroin hydrogels with bone mesenchymal stem cells (Fig. 5.19A) were used to enhance functional outcomes after cortical stroke in mice. Evidence of cortical plasticity, linked to active recovery occurring late after treatment (Fig. 5.19B), was reported in previous works [138,140,]. Brain remapping and sustained recovery were experimentally favored using a stem cell−silk fibroin biomaterial.

The recovery of injured nervous tissue, one of the main goals for regenerative therapeutic approaches, is often hindered by the limited axonal regeneration ability of the central nervous system. In this regard, looking for scaffolds that support the reconstruction of functional neuronal tissues and guide the alignment of regenerating neurons is a significant challenge in tissue engineering. Such scaffolds would promote and drive axonal growth, a crucial phase for restoring neuronal connections and, consequently, nerve function. In this topic, silk fibers have been used to exploit its outstanding features as a biomaterial to promote axonal regeneration.

The feasibility of using regenerated silk fibers − obtained through SFS − to serve as scaffolds for inducing and guiding the axonal growth was reported [139]. These fibers were shown to promote the spontaneous organization of dissociated primary cortical cells into highly interconnected cellular spheroid-like tissue formations (Fig. 5.19C−G). Neuronal projections (i.e., axons) from these cellular spheroids span hundreds of microns along the SFS fibers that act as guides and allow the connection of distant cellular spheroids. In addition, regenerated SFS fibers exhibit their potential as scaffolds to promote guidance and axonal outgrowth. Moreover, the biocompatibility of such regenerated SFS fibers allows their implantation *in vivo*, opening a new approach for developing neural tissue regeneration therapies.

Adult frogs can regrow a leg if they are treated with a device containing a silk gel (from *B. mori*) infused with five regenerative chemicals. The new limbs can apparently move and sense as well as the original legs [141].

Also, spider silk—in its native or regenerated form [142]—has become a good material for tissue engineering scaffolds.

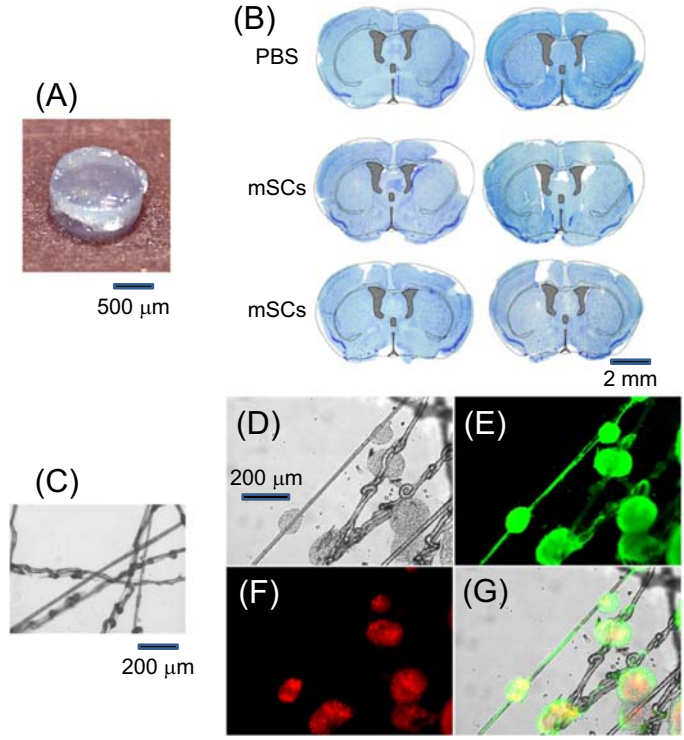

FIGURE 5.19 (A) Hydrogel of silk fibroin. (B) Images illustrating the neuroprotective effect of transplanted mesenchymal stem cells (mSCs) engrafted into silk fibroin hydrogels in mice after stroke; the images show Nissl-stained coronal brain sections performed 10 weeks after injection of PBS, mSCs alone or mSCs encapsulated in silk-fibroin hydrogels (images obtained from two different mice in each group) [138]. Note how most of the cortical territory was preserved in stroke mice coinjected with mSCs and silk fibroin gels. (C) Transmitted light images of SFS silk-fibroin fibers placed on a glass coverslip. (D–G) Immunofluorescence staining of cortical cells grown on SFS silk-fibroin fibers: transmitted light (D) and fluorescence (E and F) images of neural cortical cells cultured for 7 days on SFS fibers and stained for β-III-tubulin (E) and glial fibrillary acidic protein (F). (G) Merged image of (D − F) [139].

Constructs made with decellularized vein grafts filled with spider silk fibers (from *N. clavipes*) as nerve guidance showed complete biodegeneration over time without challenging tissue reaction. Such constructs were used to successfully bridge a 6.0 cm tibial nerve defect in adult sheep [143]. Spider silk (from *N. edulis*) has been used as a biocompatible, very stable carrier matrix combined with a collagen type I hydrogel and adipose-derived stromal cells. With such a construct, a tendon-like tissue was produced by axial strain [144].

Regenerated spider silk proteins (RSSP) are also an ideal substrate for fabricating biomedical composites for nerve tissue engineering. A fibrous composite based on RSSP from *Acallodes ventricosus*, was effective at bridging 2.0 cm sciatic nerve gap in adult rats within 10 months [145].

Acknowledgments

This study was partially funded by the Ministerio de Ciencia e Innovación (PID2020−116403RB-I00; MCIN/AEI/10.13039/501100011033) and by Comunidad de Madrid (Spain) through grants Tec4Bio-CM/P2018/NMT-4443 and MINA-CM P2022-BMD-7236. Additional funding was received from the Fondo Europeo de Desarrollo Regional (FEDER) as the response of the EU to the COVID-19 pandemic through the COVITECH-CM project.

References

[1] Craig CL, Hsu M, Kaplan D, Pierce NE. A comparison of the composition of silk proteins produced by spiders and insects. Int J Biol Macromol 1999;24(2/3):109−18.
[2] Craig CL. Evolution of arthropods silks. Annu Rev Entomol 1997;42(1):231−67.
[3] Lucas F, Shaw JTB, Smith SG. The chemical constitution of some silk fibroins and its bearing on their physical properties. J Text Inst 1955;46:440−52.
[4] Kaplan DL, Lombardi S, Muller WS, Fossey SA. Biomaterials. Novel materials from biological sources. New York: Stockton Press; 1991.
[5] Xia QY, Zhou ZY, Lu C, Cheng DJ, Dai FY, Li B, et al. A draft sequence for the genome of the domesticated silkworm (*Bombyx mori*). Science 2004;306(5703):1937−40.
[6] Xu M, Lewis RV. Structure of a protein superfiber − spider dragline silk. Proc Natl Acad Sci U S A 1990;87(18):7120−4.
[7] Rudall KM, Kenchington W. Arthropod silks the problem of fibrous proteins in animal tissues. Annu Rev Entomol 1971;16:73−96.
[8] Gatesy J, Hayashi C, Motriuk D, Woods J, Lewis R. Extreme diversity, conservation, and convergence of spider silk fibroin sequences. Science 2001;291(5513):2603−5.
[9] Blackledge TA, Pérez-Rigueiro J, Plaza GR, Perea B, Navarro A, Guinea GV, et al. Sequential origin in the high-performance properties of orb spider dragline silk. Sci Rep 2012;2(2):782.
[10] Plaza GR, Corsini P, Marsano E, Pérez-Rigueiro J, Biancotto L, Elices M, et al. Old silks endowed with new properties. Macromolecules 2009;42(22):8977−82.
[11] Vollrath F, Knight DP. Structure and function of the silk production pathway in the spider Nephila edulis. Int J Biol Macromol 1999;24(2−3):243−9.
[12] Iizuka E. Silk thread − mechanism of spinning and its mechanical properties. Appl Polym Symp 1985;41:173−85.
[13] Asakura T, Kaplan DL. Silk production and processing. In: Arntzen C, editor. Encyclopedia of agricultural science. New York: Academic Press, Inc; 1994. p. 1−11.
[14] Heim M, Keerl D, Scheibel T. Spider silk: from soluble protein to extraordinary fiber. Angew Chem Int Ed Engl 2009;48(20):3584−96.
[15] Vollrath F, Knight DP. Liquid crystalline spinning of spider silk. Nature 2001;410(6828):541−8.
[16] Jin HJ, Kaplan DL. Mechanism of silk processing in insects and spiders. Nature 2003;424(6952):1057−61.
[17] Askarieh G, Hedhammar M, Nordling K, Saenz A, Casals C, Rising A, et al. Self-assembly of spider silk proteins is controlled by a pH-sensitive relay. Nature 2010;465:236−9.
[18] Hagn F, Eisoldt L, Hardy JG, Vendrely C, Coles M, Scheibel T, et al. A conserved spider silk domain acts as a molecular switch that controls fibre assembly. Nature 2010;465:239−42.

[19] Ortlepp C, Gosline J. Consequences of forced silking. Biomacromolecules 2004;5 (3):727–31.
[20] Pérez-Rigueiro J, Elices M, Plaza G, Real JI, Guinea GV. The effect of spinning forces on spider silk properties. J Exp Biol 2005;208(14):2633–9.
[21] Shao ZZ, Vollrath F. Materials: Surprising strength of silkworm silk. Nature 2002;418 (6899):741.
[22] Pérez-Riguero J, Elices M, Llorca J, Viney C. Tensile properties of Argiope trifasciata drag line silk obtained from the spider's web. J Appl Polym Sci 2001;82(9):2245–51.
[23] Vollrath F. Spider webs and silks. Sci Am 1992;266(3):70–6.
[24] Marsh RE, Corey RB, Pauling L. An investigation of the structure of silk fibroin. Biochim Biophys Acta 1955;16(1):1–34.
[25] Martel A, Burghammer M, Davies RJ, Riekel C. Thermal behavior of *Bombyx mori* silk: evolution of crystalline parameters, molecular structure, and mechanical properties. Biomacromolecules 2007;8:3548–56.
[26] Riekel C, Branden C, Craig C, Ferrero C, Heidelbach F, Muller M. Aspects of X-ray diffraction on single spider fibers. Int J Biol Macromol 1999;24(2–3):179–86.
[27] Rousseau M, Lefevre T, Pezolet M. Conformation and orientation of proteins in various types of silk fibers produced by *Nephila clavipes* spiders. Biomacromolecules 2009;10 (10):2945–53.
[28] Work RW. Dimensions, birefringences, and force-elongation behavior of major and minor ampullate silk fibers from orb-web-spinning spiders – effects of wetting on these properties. Text Res J 1977;47(10):650–62.
[29] Pérez-Rigueiro J, Viney C, Llorca J, Elices M. Mechanical properties of silkworm silk in liquid media. Polymer 2000;41(23):8433–9.
[30] Termonia Y. Molecular modelling of the stress/strain behaviour of spider dragline. In: Elices M, editor. Structural biological materials. Amsterdam: Pergamon Press; 2000. p. 335–49.
[31] Yang ZT, Liivak O, Seidel A, Laverde G, Zax DB, Jelinski LW. Supercontraction and backbone dynamics in spider silk: C-13 and H-2 NMR studies. J Am Chem Soc 2000;122 (37):9019–25.
[32] Elices M, Plaza GR, Pérez-Rigueiro J, Guinea GV. The hidden link between supercontraction and mechanical behavior of spider silks. J Mech Behav Biomed Mater 2011;4:658–69.
[33] Pérez-Rigueiro J, Plaza GR, Torres FG, Hijar A, Hayashi C, Perea GB, et al. Supercontraction of dragline silk spun by lynx spiders (Oxyopidae). Int J Biol Macromol 2010;46:555–7.
[34] Plaza GR, Pérez-Rigueiro J, Riekel C, Perea GB, Agulló-Rueda F, Burghammer M, et al. Relationship between microstructure and mechanical properties in spider silk fibers: two regimes in the microstructural changes. Soft Matter 2012;8:6015–26.
[35] Du N, Liu XY, Narayanan J, Li LA, Lim MLM, Li DQ. Design of superior spider silk: from nanostructure to mechanical properties. Biophys J 2006;91(12):4528–35.
[36] Miller LD, Putthanarat S, Eby RK, Adams WW. Investigation of the nanofibrillar morphology in silk fibers by small angle X-ray scattering and atomic force microscopy. Int J Biol Macromol 1999;24(2/3):159–65.
[37] Glisovic A, Thieme J, Guttmann P, Salditt T. Transmission X-ray microscopy of spider dragline silk. Int J Biol Macromol 2007;40(2):87–95.
[38] Pérez-Rigueiro J, Elices M, Plaza GR, Guinea GV. Similarities and differences in the supramolecular organization of silkworm and spider silk. Macromolecules 2007;40 (15):5360–5.

[39] Poza P, Pérez-Rigueiro J, Elices M, Llorca J. Fractographic analysis of silkworm and spider silk. Eng Fract Mech 2002;69(9):1035–48.
[40] Sapede D, Seydel T, Forsyth VT, Koza MA, Schweins R, Vollrath F, et al. Nanofibrillar structure and molecular mobility in spider dragline silk. Macromolecules 2005;38(20):8447–53.
[41] Yang Z, Grubb DT, Jelinski LW. Small-angle X-ray scattering of spider dragline silk. Macromolecules 1997;30(26):8254–61.
[42] Vollrath F. General-properties of some spider silks. In: Kaplan D, Adams WW, Farmer B, Viney C, editors. ACS symposium series 544. Washington, DC: American Chemical Society; 1994. p. 17–28.
[43] Guinea GV, Pérez-Rigueiro J, Plaza GR, Elices M. Volume constancy during stretching of spider silk. Biomacromolecules 2006;7(7):2173–7.
[44] Pérez-Rigueiro J, Elices M, Llorca J, Viney C. Tensile properties of silkworm silk obtained by forced silking. J Appl Polym Sci 2001;82(8):1928–35.
[45] Guinea GV, Elices M, Pérez-Rigueiro J, Plaza GR. Stretching of supercontracted fibers: a link between spinning and the variability of spider silk. J Exp Biol 2005;208(1):25–30.
[46] Elices M, Plaza GR, Arnedo MA, Pérez-Rigueiro J, Torres FG, Guinea GV. Mechanical behaviour of silk during the evolution of orb-web spinning spiders. Biomacromolecules 2009;10(7):1904–10.
[47] Swanson BO, Blackledge TA, Beltran J, Hayashi CY. Variation in the material properties of spider dragline silk across species. Appl Phys A-Mater Sci Process 2006;82(2):213–18.
[48] Pérez-Rigueiro J, Viney C, Llorca J, Elices M. Mechanical properties of single-brin silkworm silk. J Appl Polym Sci 2000;75(10):1270–7.
[49] Fibers and fibre assemblies. In: Weidmann G, Lewis P, Reid N, editors. Structural materials. Butterworths: The Open University; 1990. Chapter 6.
[50] Elices M, Pérez-Rigueiro J, Plaza GR, Guinea GV. Finding inspiration in Argiope trifasciata spider silk fibers. JOM 2005;57(2):60–6.
[51] Yang Y, Chen X, Shao ZZ, Zhou P, Porter D, Knight DP, et al. Toughness of spider silk at high and low temperatures. Adv Mater 2005;17(1):84–8.
[52] Garrido MA, Elices M, Viney C, Pérez-Rigueiro J. Active control of spider silk strength: comparison of drag line spun on vertical and horizontal surfaces. Polymer 2002;43(4):1537–40.
[53] Garrido MA, Elices M, Viney C, Pérez-Rigueiro J. The variability and interdependence of spider drag line tensile properties. Polymer 2002;43(16):4495–502.
[54] Madsen B, Shao ZZ, Vollrath F. Variability in the mechanical properties of spider silks on three levels: interspecific, intraspecific and intraindividual. Int J Biol Macromol 1999;24(2–3):301–6.
[55] Pérez-Rigueiro J, Viney C, Llorca J, Elices M. Silkworm silk as an engineering material. J Appl Polym Sci 1998;70(12):2439–47.
[56] Pérez-Rigueiro J, Elices M, Llorca J, Viney C. Effect of degumming on the tensile properties of silkworm (*Bombyx mori*) silk fiber. J Appl Polym Sci 2002;84(7):1431–7.
[57] Cenis JL, Madurga R, Aznar-Cervantes SD, Lozano-Pérez AA, Marí-Buye N, Meseguer-Olmo L, et al. Mechanical behaviour and formation process of silkworm silk gut. Soft Matter 2015;11(8981):2015. Available from: https://doi.org/10.1039/c5sm01877c.
[58] Jiang P, Marí N, Arroyo-Hernández M, Solanas C, Gañán A, Daza R, et al. Spider silk gut: development and characterization of a novel strong spider silk fiber. Sci Rep 2014;4:7326 10.1038/srep07326.

[59] Ruiz V, Jiang P, Müller C, Jorge I, Vázquez J, Ridruejo A, et al. Preparation and characterization of *Nephila clavipes* tubuliform silk gut. Soft Matter 2019;15:1960. Available from: https://doi.org/10.1039/c9sm00212j.

[60] Pérez-Rigueiro J, Ruiz V, Cenis JL, Elices M, Guinea GV. Lessons from spider and silkworm silk guts. Front Mater 2020;. Available from: https://doi.org/10.3389/fmats.2020.00046.

[61] Gosline JM, Denny MW, Demont ME. Spider silk as rubber. Nature 1984;309 (5968):551–2.

[62] Plaza GR, Guinea GV, Pérez-Rigueiro J, Elices M. Thermo-hygromechanical behavior of spider dragline silk: glassy and rubbery states. J Polym Sci Part B-Polym Phys 2006;44 (6):994–9.

[63] Elices M, Pérez-Rigueiro J, Plaza G, Guinea GV. Recovery in spider silk fibers. J Appl Polym Sci 2004;92(6):3537–41.

[64] Madurga R, Plaza GR, Blackledge TA, Guinea GV, Elices M, Pérez-Rigueiro J. Material properties of evolutionary diverse spider silks described by variation in a single structural parameter. Sci Rep 2016;6:18991. Available from: https://doi.org/10.1038/srep18991.

[65] Garrote J, Ruiz V, Troncoso OP, Torres FG, Arnedo M, Elices M, et al. Application of the Spider Silk Standardization Initiative (S3I) methodology to the characterization of major ampullate gland silk fibers spun by spiders from Pantanos de Villa wetlands (Lima, Peru). J Mech Behav Biomed Mater 2020;111:104023. Available from: https://doi.org/10.1016/j.jmbbm.2020.104023.

[66] Blamires S, Lozano-Picazo P, Bruno, Augusto L, Arnedo M, Ruiz-León Y, et al. The Spider Silk Standardization Initaitive (S3I): a powerful tool to harness biological variability and to systematize the characterization of major ampullate silk fibers spun by spiders from suburban Sydney, Austrialia. J Mech Behav Biomed Mater 2023;140(105729):1–7.

[67] Madurga R, Blackledge TA, Perea B, Plaza GR, Riekel C, Burghammer M, et al. Persistence and variation in microstructural design during the evolution of spider silk. Sci Rep 2015;5:14820. Available from: https://doi.org/10.1038/srep14820.

[68] Tarakanova A, Buehler MJ. A materiomics approach to spider silk: protein molecules to webs. JOM 2012;64(2):214–25.

[69] Gronau G, Krishnaji ST, Kinahan ME, Giesa T, Wong JY, Kaplan DL, et al. A review of combined experimental and computational procedures for assessing biopolymer structure-process-property relationships. Biomaterials 2012;33(33):8240–55.

[70] J.O. Warwicker Comparative studies of fibroins: II. The crystal structures of various fibroins. J Mol Biol 1960;2:350–362. Available from: https://doi.org/10.1016/S0022-2836 (60)80046-0.

[71] Pérez-Rigueiro J, Elices M, Plaza GR, Guinea GV. Basic principles in the design of spider silk fibers. Molecules 2021;26:1794. Available from: https://doi.org/10.3390/molecules26061794.

[72] Keten S, Xu ZP, Ihle B, Buehler MJ. Nanoconfinement controls stiffness, strength and mechanical toughness of beta-sheet crystals in silk. Nat Mater 2010;9(4):359–67.

[73] Termonia Y. Molecular modeling of spider silk elasticity. Macromolecules 1994;27 (25):7378–81.

[74] Sugita Y, Okamoto Y. Replica-exchange molecular dynamics method for protein folding. Chem Phys Lett 1999;314(1–2):141–51.

[75] Keten S, Buehler MJ. Nanostructure and molecular mechanics of spider dragline silk protein assemblies. J R Soc Interface 2010;7(53):1709–21.

[76] Elices M, Guinea GV, Plaza GR, Karatzas C, Riekel C, Agullo-Rueda F, et al. Bioinspired fibers follow the track of natural spider silk. Macromolecules 2011;44 (5):1166–76.

[77] Gosline JM, Pollak CC, Guerette PA, Cheng A, Demont ME, Denny MW. Elastomeric network models for the frame and viscid silks from the orb web of the spider *Araneus diadematus*. Silk Polym 1994;544:328–41.
[78] Planas J, Guinea GV, Elices M. Constitutive model for fiber-reinforced materials with deformable matrices. Phys Rev E 2007;76(4):041903.
[79] Porter D, Vollrath F, Shao Z. Predicting the mechanical properties of spider silk as a model nanostructured polymer. Eur Phys J E 2005;16(2):199–206.
[80] Buehler MJ, Abraham FF, Gao HJ. Hyperelasticity governs dynamic fracture at a critical length scale. Nature 2003;426(6963):141–6.
[81] Porter D, Vollrath F. Nanoscale toughness of spider silk. Nano Today 2007;2(3):6.
[82] Schmitt O.H. Some interesting and useful biomimetic transforms. In: Proceedings of the third international biophysics congress, 29 August–3 September 1969; 1969. p. 297.
[83] Vollrath F, Porter D, Holland C. There are many more lessons still to be learned from spider silks. Soft Matter 2011;7(20):9595–600.
[84] Rammensee S, Slotta U, Scheibel T, Bausch AR. Assembly mechanism of recombinant spider silk proteins. Proc Natl Acad Sci U S A 2008;105(18):6590–5.
[85] Hardy JG, Romer LM, Scheibel TR. Polymeric materials based on silk proteins. Polymer 2008;49(20):4309–27.
[86] Chawla KK. Fibrous materials. Cambridge, UK: Cambridge University Press; 1998.
[87] Yazawa S. Spinning of concentrated aqueous silk fibroin solution. J Chem Soc Jpn 1960;63:1428–30.
[88] Ishizaka H, Watanabe Y, Ishida K, Fukumoto O. Regenerated silk prepared from ortho phosphoric acid solution of fibroin. J Sericult Sci Jpn 1989;58:87–95.
[89] Xie F, Zhang HH, Shao HL, Hu XC. Effect of shearing on formation of silk fibers from regenerated *Bombyx mori* silk fibroin aqueous solution. Int J Biol Macromol 2006;38 (3–5):284–8.
[90] Matsumoto K, Uejima H, Iwasaki T, Sano Y, Sumino H. Studies on regenerated protein fibers. 3. Production of regenerated silk fibroin fiber by the self-dialyzing wet spinning method. J Appl Polym Sci 1996;60(4):503–11.
[91] Trabbic KA, Yager P. Comparative structural characterization of naturally- and synthetically-spun fibers of *Bombyx mori* fibroin. Macromolecules 1998;31(2):462–71.
[92] Liivak O, Blye A, Shah N, Jelinski LW. A microfabricated wet-spinning apparatus to spin fibers of silk proteins. Structure–property correlations. Macromolecules 1998;31 (9):2947–51.
[93] Yao JM, Masuda H, Zhao CH, Asakura T. Artificial spinning and characterization of silk fiber from *Bombyx mori* silk fibroin in hexafluoroacetone hydrate. Macromolecules 2002;35(1):6–9.
[94] Um IC, Ki CS, Kweon HY, Lee KG, Ihm DW, Park YH. Wet spinning of silk polymer – II. Effect of drawing on the structural characteristics and properties of filament. Int J Biol Macromol 2004;34(1–2):107–19.
[95] Ha SW, Tonelli AE, Hudson SM. Structural studies of Bombyx mori silk fibroin during regeneration from solutions and wet fiber spinning. Biomacromolecules 2005;6 (3):1722–31.
[96] Phillips D, Drummy L, Conrady D, Fox D, Naik R, Stone M, et al. Dissolution and regeneration of *Bombyx mori* silk fibroin using ionic liquids. J Am Chem Soc 2004;126 (44):14350–1.
[97] Phillips D, Drummy L, Naik R, de Long H, Fox D, Trulove P, et al. Regenerated silk fiber wet spinning from an ionic liquid solution. J Mater Chem 2005;15(39):4206–8.

[98] Marsano E, Corsini P, Arosio C, Boschi A, Mormino M, Freddi G. Wet spinning of *Bombyx mori* silk fibroin dissolved in N-methyl morpholine N-oxide and properties of regenerated fibres. Int J Biol Macromol 2005;37(4):179–88.

[99] Corsini P, Pérez-Rigueiro J, Guinea GV, Plaza GR, Elices M, Marsano E, et al. Influence of the draw ratio on the tensile and fracture behavior of NMMO regenerated silk fibers. J Polym Sci Part B-Polym Phys 2007;45:2568–79.

[100] Corsini P. New fibres based on natural polymers: silk and cellulose [PhD thesis]. Genova: Universita degli Studi di Genova; 2008.

[101] Yan JP, Zhou GQ, Knight DP, Shao ZZ, Chen X. Wet-spinning of regenerated silk fiber from aqueous silk fibroin solution: discussion of spinning parameters. Biomacromolecules 2010;11(1):1–5.

[102] Zhu ZH, Ohgo KS, Watanabe R, Takezawa T, Asakura TS. Preparation and characterization of regenerated *Bombyx mori* silk fibroin fiber containing recombinant cell-adhesive proteins; nonwoven fiber and monofilament. J Appl Polym Sci 2008;109(5):2956–63.

[103] Plaza GR, Corsini P, Marsano E, Pérez-Rigueiro J, Elices M, Riekel C, et al. Correlation between processing conditions, micro-structure and mechanical behavior in regenerated silkworm silk fibers. J Polym Sci Part B-Polym Phys 2012;50(7):455–65.

[104] Pérez-Rigueiro J, Biancotto L, Corsini P, Marsano E, Elices M, Plaza GR, et al. Supramolecular organization of regenerated silkworm silk fibers. Int J Biol Macromol 2009;44(2):195–202.

[105] Pérez-Rigueiro J, Madurga R, Gañán-Calvo AM, Elices M, Guinea GV, Tasei Y, et al. Emergence of supercontraction in regenerated silkworm (*Bombyx mori*) silk fibers. Sci Rep 2019;9:2398. Available from: https://doi.org/10.1038/s41598-019-38712-6.

[106] Madurga R, Guinea GV, Elices M, Pérez-Rigueiro J, Gañán-Calvo AM. Straining flow spinning: simplified model of a bioinspired process to mass produce regenerated silk fibers controllably. Eur Polym J 2017;97:26–39 doi.org/10.1016/j.eurpolymj.2017.09.037.

[107] Pérez-Rigueiro J, Madurga R, Gañán-Calvo AM, Plaza GR, Elices M, López PA, et al. Straining flow spinning of artificial silk fibers: a review. Biomimetics 2018;3(4):29. Available from: https://doi.org/10.3390/biomimetics3040029.

[108] Madurga R, Gañán-Calvo AM, Plaza GR, Guinea GV, Elices M, Pérez-Rigueiro J. Production of high-performance bioinspired silk fibers by straining flow spinning. Biomacromolecules 2017;18(4):1127–33. Available from: https://doi.org/10.1021/acs.biomac.6b01757.

[109] Madurga R, Gañán-Calvo AM, Plaza GR, Guinea GV, Elices M, Pérez-Rigueiro J. Straining flow spinning: production of regenerated silk fibers under a wide range of mild coagulating chemistries. Green Chem 2017;19:3380. Available from: https://doi.org/10.1039/c7gc01254c.

[110] Madurga R, Gañán-Calvo AM, Plaza GR, Atienza JM, Guinea GV, Elices M, et al. Comparison of the effects of post-spinning drawing and wet stretching on regenerated silk fibers produced through straining flow spinning. Polymer 2018;150:311–17. Available from: https://doi.org/10.1016/j.polymer.2018.07.042.

[111] Madurga R, Gañán-Calvo AM, Mariscal T, Plaza GR, Guinea GV, Elices M, et al. Production of regenerated silkworm silk fibers from aqueous dopes through straining flow spinning. Text Res J 2019;89(21–22):4554–67. Available from: https://doi.org/10.1177/0040517519838050.

[112] Lazaris A, Arcidiacono S, Huang Y, Zhou JF, Duguay F, Chretien N, et al. Spider silk fibers spun from soluble recombinant silk produced in mammalian cells. Science 2002;295(5554):472–6.

[113] Teule F, Miao Y, Sohn B, Kim Y, Hull JJ, Fraser Jr. MJ, et al. Silkworms transformed with chimeric silkworm/spider silk genes spin composite silk fibers with improved mechanical properties. Proc Natl Acad Sci U S A 2012;109(3):923–8.
[114] Huemmerich D, Scheibel T, Vollrath F, Cohen S, Gat U, Ittah S. Novel assembly properties of recombinant spider dragline silk proteins. Curr Biol 2004;14(22):2070–4.
[115] Eisoldt L, Thamm C, Scheibel T. Review the role of terminal domains during storage and assembly of spider silk proteins. Biopolymers 2012;97(6):355–61.
[116] Prince JT, McGrath KP, Digirolamo C, Kaplan DL. Construction, cloning, and expression of synthetic genes encoding spider dragline silk. Biochemistry 1995;34:10879–84.
[117] Fahnestock SR, Irwin SL. Synthetic spider dragline silk proteins and their production in *Escherichia coli*. Appl Microbiol Biotechnol 1997;47(1):23–32.
[118] Fahnestock SR, Bedzyk LA. Production of synthetic spider dragline silk protein in Pichia pastoris. Appl Microbiol Biotechnol 1997;47(1):33–9.
[119] Fukushima Y. Genetically engineered syntheses of tandem repetitive polypeptides consisting of glycine-rich sequence of spider dragline silk. Biopolymers 1998;45(4):269–79.
[120] Scheller J, Guhrs KH, Grosse F, Conrad U. Production of spider silk proteins in tobacco and potato. Nat Biotechnol 2001;19(6):573–7.
[121] Wang J, Fan T, Li Xi, Hu X, Huang W, Yuan W, et al. Artificial superstrong silkworm silk surpasses natural spider silks. Matter 2022;5:4396–406. Available from: https://doi.org/10.1016/j.matt.2022.08.028.
[122] Lewicka M, Hermanson O, Rising AU. Recombinant spider silk matrices for neural stem cell cultures. Biomaterials 2012;33(31):7712–17.
[123] Scheibel T. Spider silks: recombinant synthesis, assembly, spinning, and engineering of synthetic proteins. Microb Cell Fact 2004;3:14.
[124] Chung H, Kim TY, Lee SY. Recent advances in production of recombinant spider silk proteins. Curr Opin Biotechnol 2012;23(6):957–64.
[125] Lock R.L. Process for making silk fibroin fibers. US Patent 5252285; 1993.
[126] Savage KN, Gosline JM. The effect of proline on the network structure of major ampullate silks as inferred from their mechanical and optical properties. J Exp Biol 2008;211(12):1937–47.
[127] Teule F, Addison B, Cooper AR, Ayon J, Henning RW, Benmore CJ, et al. Combining flagelliform and dragline spider silk motifs to produce tunable synthetic biopolymer fibers. Biopolymers 2012;97(6):418–31.
[128] Johar N, Khodaei A, Samadikuchaksaraei A, Reis RL, Kundu SC, Lorenzo M. Ancient fibrous biomaterials from silkworm protein fibroin and spider silk blends: biomechanical patterns. Acta Biomater 2022;153:38–67.
[129] Naskar D, Sapru S, Ghosh AK, Reis RL, Dey T, Kundu SC. Nonmulberry silk proteins: multipurpose ingredient in bio-functional assembly. Biomed Mater 2021;16(6):062002.
[130] Holland C, Numata K, Rnjak-Kovacina J, Seib FP. The biomedical use of silk: past, present, future. Adv Healthc Mater 2019;8(1). Available from: https://doi.org/10.1002/adhm.201800465.
[131] Tandon S, Kandasubramanian B, Ibrahim SM. Silk-based composite scaffolds for tissue engineering applications. Ind Eng Chem Res 2020;59(40):17593–611. Available from: https://doi.org/10.1021/acs.iecr.0c02195.
[132] Yonesi M, García-Nieto M, Guinea GV, Panetsos F, Pérez-Rigueiro J, González-Nieto D. Silk fibroin: an ancient material for repairing the injured nervous system. Pharmaceutics 2021;13:429. Available from: https://doi.org/10.3390/pharmaceutics13030429.

[133] Zhang L, Zhang W, Hu W, Fei Y, Liu H, Huang Z, et al. Systematic review of silk scaffolds in musculoskeletal tissue engineering applications in the recent decade. ACS Biomater Sci Eng 2021;7(3):817−40. Available from: https://doi.org/10.1021/acsbiomaterials.0c01716.

[134] Leng-Duei K, Yuan C, Choon-Peng T, Yin-Win K, Xian-Jun L, Si-Yin T, et al. Structures, mechanical properties and applications of silk fibroin materials. Prog Polym Sci 2015;46:86−110. Available from: https://doi.org/10.1016/j.progpolymsci.2015.02.001.

[135] Li G, Sun S. Silk fibroin-based biomaterials for tissue engineering applications. Molecules 2022;27(9):2757. Available from: https://doi.org/10.3390/molecules27092757.

[136] Enomoto S, Sumi M, Kajimoto K, Nakazawa Y, Takahashi R, Takabayashi C, et al. Long-term patency of small-diameter vascular graft made from fibroin, a silk-based biodegradable material. J Vasc Surg 2010;51(1):155−64.

[137] Das S, Sharma M, Saharia D, Sarma KK, Sarma MG, Borthakur BB, et al. In vivo studies of silk based gold nano-composite conduits for functional peripheral nerve regeneration. Biomaterials 2015;62:66−75. Available from: https://doi.org/10.1016/j.biomaterials.2015.04.047.

[138] Fernández-García L, Pérez-Rigueiro J, Martinez-Murillo R, Panetsos F, Ramos M, Guinea GV, et al. Cortical reshaping and functional recovery induced by silk fibroin hydrogels-encapsulated stem cells implanted in stroke animals. Front Cell Neurosci 2018;12(296):29. Available from: https://doi.org/10.3389/fncel.2018.00296.

[139] Mercado J, Pérez-Rigueiro J, González-Nieto D, Lozano-Picazo P, López P, Panetsos F, et al. Regenerated silk fibers obtained by straining flow spinning for guiding axonal elongation in primary cortical neurons. ACS Biomater Sci Eng 2020;6(12):6842−52. Available from: https://doi.org/10.1021/acsbiomaterials.0c00985.

[140] Fernández-García L, Marí-Buyé N, Barios JA, Madurga M, Elices M, Pérez-Rigueiro J, et al. Safety and tolerability of silk fibroin hydrogels implanted into the mouse brain. Acta Biomater 2016;45:262−75. Available from: https://doi.org/10.1016/j.actbio.2016.09.003.

[141] Murugan NJ, Vigran HJ, Miller KA, Golding A, Pham QL, Sperry MM, et al. Acute multidrug delivery via a wearable bioreactor facilitates long-term limb regeneration and functional recovery in adult Xenopus laevis. Sci Adv 2022;8(4). Available from: https://doi.org/10.1126/sciadv.abj2164.

[142] Bittencourt DMdC, Oliveira P, Michalczechen-Lacerda VA, Rosinhg GMS, Jones JA, Rech EL. Biogineering of spider silks for the production of biomedical materials. Front Bioeng Biotechnol 2022;10:958486. Available from: https://doi.org/10.3389/fbioe.2022.958486.

[143] Radtke C, Allmeling C, Waldmann KH, Reimers K, Thies K, Schenk HC, et al. Spider silk constructs enhance axonal regeneration and remyelination in long nerve defects in sheep. PLoS One 2011;. Available from: https://doi.org/10.1371/journal.pone.0016990.

[144] Schlottmann F, Strauss S, Plaass C, Welke B, Vogt PM, Kuhbier JW. Spider silk-augmented scaffolds and adipose-derived stromal cells loaded with uniaxial cyclic strain: first investigations of a novel approach for tendon-like constructs. Appl Sci 2021;11(3):1218. Available from: https://doi.org/10.3390/app11031218.

[145] Zhang H, Wang K, Xing Y, Yua Q. Lysine-doped polypyrrole/spider silk protein/poly(l-lactic) acid containing nerve growth factor composite fibers for neural application. Mater Sci Eng C 2015;56(1):564−73.

WOODHEAD PUBLISHING SERIES IN BIOMATERIALS

Extensively covers the structure, properties, processing methods, and biomedical applications of silk-based biomaterials

Key features

- Covers all key silk biomaterial types, including mulberry, Bombyx mori and non-mulberry/wild silk protein fibroins, sericins, and spider silk, as well as their composite blends and various structures and scaffold platforms
- Describes the cutting-edge processing techniques for each silk type, from traditional
  to nonconventional methods, such as using ionic liquids and engineering nanofibers
  and other biomedical matrices
- Explores a range of applications in tissue engineering, regenerative, and precision medicine, including bioprinting, bioelectronics, and medical devices

Silk-based Biomaterials for Tissue Engineering, Regenerative and Precision Medicine*, *Second Edition is a must-have reference which comprehensively covers silk-based biomaterials and their importance in translational uses and biomedicine. This new edition considers the progress made in the last 8 years and holistically reviews the types, structure and properties, processing methods, and specific biomedical applications for silk-based biomaterials. Many new chapters are featured, including a discussion of cutting-edge fabrication methods and techniques, new and improved blends/composites, and an expanded range of applications in tissue engineering, regenerative, and precision medicine.

Silk-based Biomaterials for Tissue Engineering, Regenerative and Precision Medicine*, *Second Edition is a vital resource for materials and tissue engineering scientists, R&D departments in industry and academia, and academics interested in biomaterials, regenerative, and precision medicine.

About the Editors

Subhas C. Kundu, PhD, is a research coordinator and former European Research Area Chair at the 3B's Research Group, I3Bs—Institute on Biomaterials, Biodegradables and Biomimetics of the University of Minho (Portugal).

Rui L. Reis, PhD, DSc, Honoris Causa MD, Honoris Causa PhD, FBSE, FTERM, is a full professor and dean/president of I3Bs—Institute on Biomaterials, Biodegradables and Biomimetics, founding director of the 3B's Research Group, and director of the PT Government ICVS/3B's Associate Laboratory (Portugal). He is the CEO of the European Institute of Excellence on Tissue Engineering and Regenerative Medicine.

ELSEVIER
WP
WOODHEAD PUBLISHING
An imprint of Elsevier
elsevier.com/books-and-journals

ISBN 978-0-323-96017-5
9 780323 960175